Development of a two-fluid model for dynamic multiphase pipeline simulations

Introduction and description of the prototype code Rosa

Restricted
SR.16.10592
March 2016

Restricted **SR.16.10592**

Development of a two-fluid model for dynamic multiphase pipeline simulations

Introduction and description of the prototype code Rosa

by

B. Sanderse (PTE/EPFA)

Shell Global Solutions International B.V., Amsterdam

Further electronic copies can be obtained from the Global Information Centre.

Executive Summary

In this report we describe the development of a discretization method for the two-fluid model. This one-dimensional two-fluid model describes stratified multiphase flow in pipelines. It is the basis for codes such as OLGA (the current industry standard) and LedaFlow. Compas, Shell's in-house simulator, uses a simplified version of the two-fluid model, namely the drift-flux model, which contains less physics than the two-fluid model. The main purpose of this work is to investigate how to discretize the two-fluid model so that it can be incorporated into a future version of Compas.

A second order finite volume discretization of the two-fluid model on a staggered grid is proposed, with the second order time integration scheme BDF2, the Backward Difference Formula method that uses two previous time levels. An eigenvalue analysis shows under which conditions the two-fluid model is well-posed and when it is stable. We have coded the numerical discretization and solver for the two-fluid model in a Matlab tool called *Rosa*. Numerical tests with interfacial waves developing into slugs (Kelvin-Helmholtz instabilities) confirm the stability analysis and confirm that the method is second order in space and time (for smooth solutions). Further tests on the dam-break problem show that shock and expansion waves are correctly present in the numerical solution and satisfy the correct jump conditions and the correct shock speed.

Besides the extension from the drift-flux to the two-fluid model, the *Rosa* code provides a new test environment in which future enhancements to Compas can be investigated. Such enhancements will be:

- Including hydraulic gradient terms in the equations. These terms are the mechanism behind the appearance of interfacial waves (Kelvin-Helmholtz instabilities).
- Replacing the volume constraint (i.e. the sum of the hold-ups equals 1) by a pressure equation in such a way that the volume error remains zero.
- Deriving a boundary treatment based on a local eigenvalue analysis of the governing equations.
- Investigating algorithms for bypass pigging, in particular the selection of friction models.
- Coupling to a reservoir model to study well-reservoir interaction.

Table of Contents

1. Introduction and background

The motion of two fluids in a pipe or channel can be approximated by the one-dimensional two-fluid model (for a derivation see example [18]). The two-fluid model is the basis for most existing dynamic multiphase pipeline simulation tools, such as OLGA (Schlumberger), LedaFlow (Total, Conocophillips, SINTEF; Kongsberg), MAST (TeaSistemi), TACITE (IFP, Total). In contrast to these, Shell's in-house code Compas currently uses a simplified version of the two-fluid model, namely the so-called drift-flux model. This means that Compas does not solve a separate momentum equation for each of the phases, but instead it solves a single momentum equation for the mixture velocity whereas the slip between the phases is represented by an algebraic correlation.

To make Compas more accurate and to bring it to the same level as commercial simulators such as OLGA and LedaFlow, the currently employed drift-flux model should be replaced by the two-fluid model. The two-fluid model is closer to the actual physics, since it is based on a momentum equation for each phase. The two-fluid model has the potential to circumvent the use of flow pattern maps [6]. For example, the growth of unstable interfacial waves in stratified flow leading to the development of slugs is captured by the two-fluid model. However, due to the one-dimensional nature, the two-fluid model can be ill-posed under certain conditions, which is (in contrast to being unstable) a non-physical effect that has to be prevented. The difference between well-posedness and stability can be confusing and this will therefore be explained below.

1.1. Stability and well-posedness of the two-fluid model

Well-posedness is determined by writing the governing equations of the two-fluid model in the quasi-linear form,

$$\boldsymbol{U}_t + \boldsymbol{A}(\boldsymbol{U})\boldsymbol{U}_x = \boldsymbol{S}(\boldsymbol{U}), \tag{1.1}$$

and determining the eigenvalues of $\boldsymbol{A}$. This is a so-called characteristic analysis. The source terms $\boldsymbol{S}$ do no contain derivatives and do not influence the well-posedness of the system. Real and distinct eigenvalues indicate a well-posed hyperbolic system of equations. If a system of equations is not well-posed, numerical 'solutions' have little meaning, and one should not expect convergence to an asymptotic state upon grid and time-step refinement.

Linear stability is investigated by linearizing the governing equations around a background state and assuming a travelling wave solution for the perturbation (periodic boundary conditions), i.e. $e^{i(\omega t - kx)}$. This results in a system of equations which possesses non-trivial solutions if the determinant vanishes, which occurs if the dispersion relation between the wavelength and the frequency, $\omega = \omega(k)$, is satisfied. If ω has an imaginary component, waves will grow (i.e. unstable behaviour) or decrease (i.e. stable behaviour) in time. Chapter 3 gives a more detailed explanation.

The available literature on stability and well-posedness of the two-fluid model can be summarized as follows:

- The 'standard' or 'basic' two-fluid model, which is the formulation without hydrostatic pressure variation (hydraulic gradients), without surface tension and without viscosity is ill-posed. This means that the system of partial differential equations does not have purely real eigenvalues. This was already shown in [17].
- An artificial interfacial pressure term can make the models unconditionally hyperbolic [7], but this is a mathematical 'trick', with little physical background. With this approach the growth of interfacial waves, due to Kelvin-Helmholtz instabilities, is not possible [8, 13].
- Including the hydrostatic variation of the pressure ('hydraulic' or 'level' gradients) makes the problem conditionally hyperbolic: if the well-known inviscid Kelvin-Helmholtz (IKH) criterion (see e.g. [1, 11, 13])

$$\Delta U^2 \leq \left(\frac{\alpha_O}{\rho_O} + \frac{\alpha_G}{\rho_G}\right) \frac{\rho_O - \rho_G}{\frac{\mathrm{d}\alpha_O}{\mathrm{d}h}} g_n \tag{1.2}$$

  is satisfied, the system of equations possesses real and distinct eigenvalues. In this case the linear stability analysis gives the same criterion as the well-posedness analysis.
- The well-posedness of the model is unchanged when viscous terms are added, because the shear stress terms do not involve differential operators. However, the stability analysis changes for the viscous case: the viscous flow becomes unstable at a lower velocity difference than the inviscid flow. In the viscous case there is a region, namely in-between the viscous Kelvin-Helmholtz (VKH) and IKH stability boundaries, where the two-fluid model is well-posed and unstable.

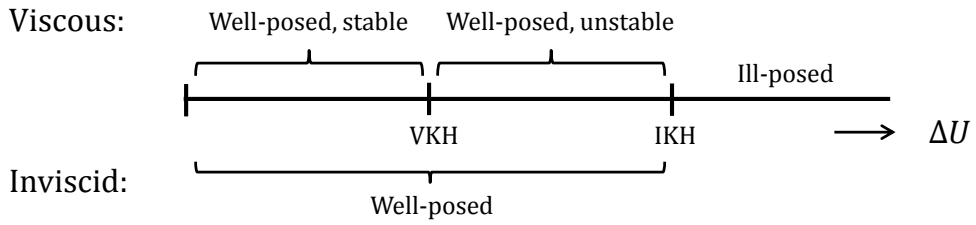

Figure 1.1: Schematic of well-posedness and stability regions for two-fluid model.

- Including surface tension makes the model unconditionally well-posed [19]. For very small scale perturbations, below a certain cut-off wavelength, the model is also stable. However, in between this cut-off wavelength and the IKH wavelength the model is unstable (though well-posed) [8]. When sufficiently fine grids are used in numerical simulations, these short-wavelength instabilities are resolved and will grow [10].

- Artificial diffusion can further stabilize the equations. Holmås [10] adds artificial (non-physical) diffusion to both mass and momentum equations and obtains a well-posed, stable model. Fullmer [8] argues to include a physical viscous term, representing molecular and turbulent viscosity, which gives nonlinear stability to long wave perturbations and shock formation. This can be seen as a constitutive model that dissipates energy as would in reality occur during wave breaking (which cannot be represented in a 1D model). The axial diffusion terms feature spatial derivatives and influence the hyperbolicity of the model, whereas the wall shear stress does not.
- Compressibility has little effect on the well-posedness of the two-fluid model [5]; the stability limit remains essentially unchanged. However, the dispersion relation $\omega(k)$ becomes quartic instead of quadratic [8].

Other considerations that will affect the hyperbolicity and stability of the model are

- The presence of a virtual mass force to account for bubble flow [14].
- The momentum flux parameter, which corrects for the one-dimensional assumption that the average of products is equals the product of averages [14].

In this report we will extend the basic two-fluid model with hydraulic gradient terms and friction terms. This is sufficient to obtain a well-posed model for some flow conditions with which the growth of interfacial waves can be simulated. We have coded the two-fluid model in a Matlab tool, and we have carried out a number of test cases.

1.2. Outline of report

This report is structured as follows. First we show the governing equations in both differential and integral form in chapter 2. Subsequently, in chapter 3 we present the analysis of stability and well-posedness of the governing equations. Chapter 4 explains the spatial discretization and chapter 5 the temporal discretization. Results for two test cases, namely the Kelvin-Helmholtz instability and the dam-break problem are presented in chapter 6.

2. Governing equations

2.1. Differential equations

The two-fluid model can be derived by considering the stratified flow of oil and gas in a pipeline [18]. The main assumptions that we make are:

- one-dimensional, stratified flow;
- compressible gas (and possibly also compressible liquid);
- isothermal flow (no energy equation required);
- hydrostatic pressure variation (simplified transverse momentum equation) is introduced via hydraulic gradients;
- no surface tension.

The resulting equations for conservation of mass and momentum are

$$\frac{\partial}{\partial t}\left(\rho_G A_G\right) + \frac{\partial}{\partial s}\left(\rho_G u_G A_G\right) = 0, \tag{2.1}$$

$$\frac{\partial}{\partial t}\left(\rho_O A_O\right) + \frac{\partial}{\partial s}\left(\rho_O u_O A_O\right) = 0, \tag{2.2}$$

$$\begin{aligned}\frac{\partial}{\partial t}\left(\rho_G u_G A_G\right) + \frac{\partial}{\partial s}(\rho_G u_G^2 A_G) = &-\frac{\partial p}{\partial s}A_G - \rho_G g_n A_G \frac{\partial h}{\partial s} \\ &- \tau_{GO} P_{GO} - \tau_G P_G - \rho_G A_G g_s,\end{aligned} \tag{2.3}$$

$$\begin{aligned}\frac{\partial}{\partial t}\left(\rho_O u_O A_O\right) + \frac{\partial}{\partial s}(\rho_O u_O^2 A_O) = &-\frac{\partial p}{\partial s}A_O - \rho_O g_n A_O \frac{\partial h}{\partial s} \\ &+ \tau_{GO} P_{GO} - \tau_O P_O - \rho_O A_O g_s,\end{aligned} \tag{2.4}$$

supplemented with the volume equation (constraint):

$$A_G + A_O = A. \tag{2.5}$$

In these equations ρ_β denotes the density of phase β (either Oil or Gas), A_β the cross-sectional area occupied by phase β, h the height of the liquid layer measured from the bottom of the pipeline with respect to the horizontal, u_β the velocity of phase β, p the pressure at the interface, τ the shear stress (wall or interfacial), g the gravitational constant, ϕ the local inclination of the pipeline, $g_n = g\cos\phi$ and $g_s = g\sin\phi$. The volume equation (2.5) is an additional equation, which cannot be derived from the conservation equations. It is a physical constraint expressing that the two fluids together exactly occupy the pipeline cross-section. In Compas the two momentum equations are added to give a total momentum equation, which is supplemented with a slip relation that describes the difference between the phase velocities.

A_G (or A_O) and h are related by a non-linear algebraic expression in case of a circular pipeline (for channel flow one simply has $h = A_O$). Similarly, the wetted and interfacial perimeters P_G, P_O and P_{GO} can be expressed as a function of the hold-up fraction or the

interface height (see [18]). We can make use of Biberg's approximation [2] to avoid the need to solve a non-linear equation, or we can choose the height h as primitive variable instead of A_O.

The second term on the right-hand side of each of the momentum equations is the 'hydraulic gradient' or 'level gradient' term. They are a result of the assumption that the pressure varies hydrostatically in vertical direction. The form displayed in equation (2.4),

$$LG_O = -\rho_O g_n A_O \frac{\partial h}{\partial s}, \quad LG_G = -\rho_G g_n A_G \frac{\partial h}{\partial s}, \tag{2.6}$$

is strictly speaking only valid for the incompressible case. In the literature, this incompressible form is also used in a compressible context, but this requires an assumption on the spatial derivatives of the density. The full compressible form is given by

$$LG_O = \frac{\partial}{\partial s}\left(\rho_O g_n \left[(R-h)A_O - \frac{1}{12}C_{\text{int}}^3\right]\right) \quad LG_G = \frac{\partial}{\partial s}\left(\rho_G g_n \left[(R-h)A_G + \frac{1}{12}C_{\text{int}}^3\right]\right), \tag{2.7}$$

and is further explained in appendix A. We propose to use this full compressible form, which is more complete than the incompressible one and has the advantage that it is in conservative form.

For simplicity, but without loss of generality, we replace the energy equation by an (isothermal) equation of state relating the density directly to the pressure:

$$\rho_G = \rho_G(p), \quad \rho_O = \rho_O(p). \tag{2.8}$$

In Compas a mixture energy equation is solved to obtain the temperature.

The interfacial and wall friction terms are modelled as follows. The wall friction is modelled as

$$\tau_G = \frac{1}{2} f_G \rho_G u_G |u_G|, \tag{2.9}$$

$$\tau_O = \frac{1}{2} f_O \rho_O u_O |u_O|, \tag{2.10}$$

where the friction factors (based on steady fully developed flow) are given by (see e.g. [1, 13]):

$$f_\beta = C_\beta \frac{1}{\text{Re}_\beta^n}, \tag{2.11}$$

and the Reynolds number is based on the hydraulic diameter:

$$\text{Re}_\beta = \frac{\rho_\beta u_\beta D_\beta}{\mu_\beta}, \tag{2.12}$$

$$D_G = \frac{4A_G}{P_G + P_{OG}}, \qquad D_O = \frac{4A_O}{P_O}. \tag{2.13}$$

The coefficients C_β and n are given by

$$C_\beta = \begin{cases} 16 \\ 0.046 \end{cases} \qquad n = \begin{cases} 1 & \text{laminar} \\ 0.2 & \text{turbulent} \end{cases}. \tag{2.14}$$

The interfacial friction is expressed in terms of the difference in velocity between the phases, and the gas density:

$$\tau_{GO} = \frac{1}{2} f_{GO} \rho_G (u_G - u_O)|u_G - u_O|, \tag{2.15}$$

where

$$f_{GO} = \begin{cases} f_G & f_G > 0.014, \\ 0.014 & f_G \leq 0.014. \end{cases} \tag{2.16}$$

Of course, other models for the friction factor are also present in the literature, but they are not the focus of the current study.

As a result, we have five equations with five unknowns (A_G, A_O, u_G, u_O, p) and one can roughly state that:

- The mass equations are equations for the evolution of A_G and A_O.
- The momentum equations are equations for the evolution of u_G and u_O.
- The volume equation is, implicitly, an equation for the pressure p.

The differential equations can be used to determine if the model is hyperbolic (i.e. it has real and distinct eigenvalues) and a linear stability analysis can be applied to investigate the growth of perturbations, such as Kelvin-Helmholtz instabilities. The integral form of the equations is more useful for developing a discretization based on the finite volume method.

A special case of the described two-fluid model occurs when the constraint and pressure gradient terms are dropped, which means that there is no interaction between the liquid and gas phase: the *shallow water equations* (SWE). They are described in appendix B and tested in section 6.2.

2.2. The incompressible flow limit

The incompressible limit is often discussed in the literature and is of interest because the phase velocities in multiphase pipelines are often much smaller than the speed of sound. However, the incompressible limit can lead to numerical challenges, similar to what is the case for the single-phase Navier-Stokes equations. In this report we will not consider incompressible flow simulations, but we give some comments on methods encountered in the literature and indicate that the incompressible limit requires careful treatment. This is a subject for possible future research.

In the incompressible limit, the densities are constant, and the mass equations in the two-fluid model can be written as

$$\frac{\partial}{\partial t}\left(A_G\right) + \frac{\partial}{\partial s}\left(u_G A_G\right) = 0, \tag{2.17}$$

$$\frac{\partial}{\partial t}\left(A_O\right) + \frac{\partial}{\partial s}\left(u_O A_O\right) = 0. \tag{2.18}$$

These can be combined with the volume equation (2.5) to give the following constraint:

$$\frac{\partial}{\partial s}\left(A_G u_G + A_O u_O\right) = 0, \tag{2.19}$$

which can be integrated in space to give

$$A u_{\text{mix}} := A_G u_G + A_O u_O = Q(t). \tag{2.20}$$

Expanding the convective terms in the momentum equations, using $\rho = const.$ and substituting the mass equations, yields

$$\frac{\partial}{\partial t}\left(\rho_G u_G A_G\right) + \frac{\partial}{\partial s}(\rho_G u_G^2 A_G) = A_G\left[\frac{\partial}{\partial t}\left(\rho_G u_G\right) + \frac{\partial}{\partial s}\left(\frac{1}{2}\rho_G u_G^2\right)\right]. \tag{2.21}$$

Dividing the gas and oil momentum equations by A_G and A_O, respectively, and combining them such that the pressure disappears, gives

$$\begin{aligned}\frac{\partial}{\partial t}\left(\rho_O u_O - \rho_G u_G\right) + \frac{\partial}{\partial s}\left(\frac{1}{2}\left(\rho_O u_O^2 - \rho_G u_G^2\right)\right) = \\ -\left(\rho_O - \rho_G\right) g_n \frac{\partial h}{\partial s} - \tau_{GO} P_{GO}\left(\frac{1}{A_O} + \frac{1}{A_G}\right) - \left(\tau_O \frac{P_O}{A_O} - \tau_G \frac{P_G}{A_G}\right) - \left(\rho_O - \rho_G\right) g_s.\end{aligned} \tag{2.22}$$

At the same time, the mass equations in their original compressible form can be combined to give

$$\frac{\partial}{\partial t}\left(\rho_G A_G + \rho_O A_O\right) + \frac{\partial}{\partial s}\left(\rho_G u_G A_G + \rho_O u_O A_O\right) = 0. \tag{2.23}$$

We now have four equations ((2.5), (2.20), (2.22), (2.23)), for four unknowns (A_G, A_O, u_G, u_O), which are in 'conservative' form [9, 15, 22]. However, the analysis above is only valid for sufficiently smooth solutions. In case shocks appear in the solution, it is necessary to work with the original equations for conservation of mass and momentum in order to obtain the correct shock speed: 'One danger to observe in dealing with conservation laws is that transforming the differential form into what appears to be an equivalent differential equation may not give an equivalent equation in the context of weak solutions' [12]. It is therefore questionable if the model of Vreenegoor et al. [21] (see also Blom et al. [4]) is correct in the presence of shock waves.

3. Stability analysis

The investigate the stability of the two-fluid model we follow [14]:

- Linearize the governing equations around a reference state (steady state): $\boldsymbol{W} = \boldsymbol{W}_0 + \delta\boldsymbol{W}$. This results in an equation for the perturbations $\delta\boldsymbol{W}$.
- Assume a travelling wave solution for the perturbations, i.e. $\delta\boldsymbol{W} = \boldsymbol{\epsilon} e^{i(\omega t - kx)}$. This gives a matrix-vector equation of the form $\boldsymbol{A}\delta\boldsymbol{W} = 0$.
- Determine the dispersion relation $\omega(k)$ from $\det(\boldsymbol{A}) = 0$.

A similar approach is taken in Liao et al. [13] and Fullmer et al. [8]. An alternative approach, taken by for example Barnea and Taitel [1], Henkes et al. [9], and also shown in Montini [14], is to combine the governing PDEs into a single PDE for the liquid height h_O. This process is somewhat cumbersome and more prone to errors, whereas the 'matrix approach' is relatively simple to apply and easily extendible to take into account viscous or compressibility effects.

3.1. Incompressible flow

We start with the incompressible situation, because it allows to compare with results from the literature. We repeat the governing equations:

$$\frac{\partial}{\partial t}\left(A_G\right) + \frac{\partial}{\partial s}\left(u_G A_G\right) = 0, \tag{3.1}$$

$$\frac{\partial}{\partial t}\left(A_O\right) + \frac{\partial}{\partial s}\left(u_O A_O\right) = 0, \tag{3.2}$$

$$\frac{\partial}{\partial t}\left(u_G A_G\right) + \frac{\partial}{\partial s}(u_G^2 A_G) = -\frac{A_G}{\rho_G}\frac{\partial p}{\partial s} - g_n A_G \frac{\partial h}{\partial s} + \frac{F_G}{\rho_G}, \tag{3.3}$$

$$\frac{\partial}{\partial t}\left(u_O A_O\right) + \frac{\partial}{\partial s}(u_O^2 A_O) = -\frac{A_O}{\rho_O}\frac{\partial p}{\partial s} - g_n A_O \frac{\partial h}{\partial s} + \frac{F_O}{\rho_O}, \tag{3.4}$$

supplemented with the volume equation (constraint):

$$A_G + A_O = A, \tag{3.5}$$

and the 'body' forces (not containing differential operators)

$$F_G = -\tau_{GO} P_{GO} - \tau_G P_G - \rho_G A_G g_s, \tag{3.6}$$

$$F_O = \tau_{GO} P_{GO} - \tau_O P_O - \rho_O A_O g_s. \tag{3.7}$$

The equations can be written in the following quasi-linear form:

$$\boldsymbol{A}(\boldsymbol{W})\frac{\partial \boldsymbol{W}}{\partial t} + \boldsymbol{B}(\boldsymbol{W})\frac{\partial \boldsymbol{W}}{\partial s} = \boldsymbol{C}(\boldsymbol{W}), \tag{3.8}$$

where

$$\boldsymbol{A} = \begin{pmatrix} 1 & 0 & 0 & 0 \\ -1 & 0 & 0 & 0 \\ u_O & A_O & 0 & 0 \\ -u_G & 0 & A_G & 0 \end{pmatrix}, \quad \boldsymbol{B} = \begin{pmatrix} u_O & A_O & 0 & 0 \\ -u_G & 0 & A_G & 0 \\ u_O^2 + g_n H_O & 2A_O u_O & 0 & A_O/\rho_O \\ -u_G^2 + g_n H_G & 0 & 2A_G u_G & A_G/\rho_G \end{pmatrix}, \tag{3.9}$$

and $\boldsymbol{C}$ contains F_G/ρ_G and F_O/ρ_O. The constraint has been used to express A_G in terms of A_O. Furthermore the hydraulic gradients are rewritten as

$$A_O \frac{\partial h}{\partial s} = A_O \frac{\partial h}{\partial A_O}\frac{\partial A_O}{\partial s} = \alpha_O \frac{\partial h}{\partial \alpha_O}\frac{\partial A_O}{\partial s} = H_O \frac{\partial A_O}{\partial s}, \tag{3.10}$$

$$A_G \frac{\partial h}{\partial s} = A_G \frac{\partial h}{\partial A_O}\frac{\partial A_O}{\partial s} = \alpha_G \frac{\partial h}{\partial \alpha_O}\frac{\partial A_O}{\partial s} = H_G \frac{\partial A_O}{\partial s}, \tag{3.11}$$

where $H_O/\alpha_O = H_G/\alpha_G = \frac{\partial h}{\partial \alpha_O}\,(= H)$. This notation is the same as used by Liao [13] and Montini [14].

We linearize the governing equations by writing $A_l = A_l^0 + \delta A_l$ (for all unknowns), using the fact that the reference state (indicated by $(.)^0$) satisfies the equations (see section 3.3), and neglecting products of disturbances. The linearized equations then read (as example we show the liquid mass and momentum equations):

$$\frac{\partial}{\partial t}(\delta A_O) + u_O^0 \frac{\partial}{\partial s}(\delta A_O) + A_O^0 \frac{\partial}{\partial s}(\delta u_O) = 0, \tag{3.12}$$

$$\begin{aligned} u_O^0 \frac{\partial}{\partial t}(\delta A_O) + A_O^0 \frac{\partial}{\partial t}(\delta u_O) + 2A_O^0 u_O^0 \frac{\partial}{\partial s}(\delta u_O) + (u_O^0)^2 \frac{\partial}{\partial s}(\delta A_O) = \\ - \frac{A_O^0}{\rho_O}\frac{\partial \delta p}{\partial s} - \frac{\delta A_O^0}{\rho_O}\frac{\partial p^0}{\partial s} - g_n H_O^0 \frac{\partial \delta A_O}{\partial s} + \frac{1}{\rho_O}\frac{\delta F_O^0}{\delta \boldsymbol{W}}\delta \boldsymbol{W}, \end{aligned} \tag{3.13}$$

where $\boldsymbol{W}$ contains the vector with unknowns: $\boldsymbol{W} = [A_O, u_O, u_G, p]^T$, and $g_n = g\cos\phi$. Note the presence of the term $\frac{\delta A_O^0}{\rho_O}\frac{\partial p^0}{\partial s}$, which is nonzero in the viscous cases, where a constant pressure gradient $\frac{\partial p^0}{\partial s}$ is needed to drive the flow. This term enters in the right-hand side of the total system of equations, which can be written in matrix-vector form as follows:

$$\boldsymbol{A}^0 \frac{\partial \delta \boldsymbol{W}}{\partial t} + \boldsymbol{B}^0 \frac{\partial \delta \boldsymbol{W}}{\partial s} = \boldsymbol{C}^0 \delta \boldsymbol{W}, \tag{3.14}$$

where $\boldsymbol{A}^0 = \boldsymbol{A}(\boldsymbol{W}^0)$, $\boldsymbol{B}^0 = \boldsymbol{B}(\boldsymbol{W}^0)$, and

$$\boldsymbol{C}^0 = \frac{\delta \boldsymbol{F}^0}{\delta \boldsymbol{W}}, \tag{3.15}$$

with $\boldsymbol{F} = [0, 0, F_G/\rho_G, F_O/\rho_O]^T$. It is cumbersome to determine $\boldsymbol{C}^0$ analytically due to the presence of the friction factors, see equation (2.11). Note that $\boldsymbol{A}^0$ and $\boldsymbol{B}^0$ are the

same as $\boldsymbol{A}$ and $\boldsymbol{B}$; this is because the nonlinearity of the equations is at most quadratic (the convective terms).

The perturbation is assumed to be of a wave like form, $\delta \boldsymbol{W} = \boldsymbol{\varepsilon} e^{i(\omega t - kx)}$. This leads to

$$\left(\boldsymbol{A}^0(i\omega) - \boldsymbol{B}^0(ik) - \boldsymbol{C}^0\right) \boldsymbol{\varepsilon} e^{i(\omega t - kx)} = 0, \tag{3.16}$$

and for non-trivial solutions we need

$$\mathrm{Det}\left(\boldsymbol{A}^0(i\omega) - \boldsymbol{B}^0(ik) - \boldsymbol{C}^0\right) = 0. \tag{3.17}$$

After some rewriting (simplifying the momentum equations with the mass equations), the determinant can be written as

$$\begin{vmatrix} i(\omega - u_O k) & -ikA_O & 0 & 0 \\ i(-\omega + u_G k) & 0 & -ikA_G & 0 \\ -ikg_n H_O + \frac{1}{\rho_O}\frac{\partial p}{\partial s} - \frac{1}{\rho_O}\frac{\delta F_O}{\delta A_O} & i(\omega A_O - kA_O u_O) - \frac{1}{\rho_O}\frac{\delta F_O}{\delta u_O} & -\frac{1}{\rho_O}\frac{\delta F_O}{\delta u_G} & -ikA_O/\rho_O \\ -ikg_n H_G - \frac{1}{\rho_G}\frac{\partial p}{\partial s} - \frac{1}{\rho_G}\frac{\delta F_G}{\delta A_O} & -\frac{1}{\rho_G}\frac{\delta F_G}{\delta u_O} & i(\omega A_G - kA_G u_G) - \frac{1}{\rho_G}\frac{\delta F_G}{\delta u_G} & -ikA_G/\rho_G \end{vmatrix} = 0. \tag{3.18}$$

This is the same as reported by Montini [14], except that he divides all equations by A and works with α_O instead of A_O. Expanding the determinant gives a quadratic equation in ω, which we solve with the software tool Mathematica. For the case of a horizontal pipeline and inviscid flow, we have $F_O = F_G = 0$ (so $\boldsymbol{C}^0 = 0$), and the solution for ω is given by

$$\omega_{1,2} = k \frac{\left(\frac{\rho_O u_O}{\alpha_O} + \frac{\rho_G u_G}{\alpha_G}\right) \pm \sqrt{\left(\frac{\rho_O}{\alpha_O} + \frac{\rho_G}{\alpha_G}\right)(\rho_O - \rho_G) H g_n - \frac{\rho_O \rho_G}{\alpha_O \alpha_G}(u_G - u_O)^2}}{\frac{\rho_O}{\alpha_O} + \frac{\rho_G}{\alpha_G}}, \tag{3.19}$$

which corresponds to the expression reported by Liao et al. [13]. The growth rate becomes imaginary if the expression under the root is negative, i.e., if

$$\Delta U^2 = (u_G - u_O)^2 > \left(\frac{\alpha_O}{\rho_O} + \frac{\alpha_G}{\rho_G}\right)(\rho_O - \rho_G) H g_n. \tag{3.20}$$

This is also the condition at which the differential equations become *ill-posed* - see equation (1.2). This is because the well-posedness (characteristic) analysis is concerned with finding eigenvalues of the system

$$\mathrm{Det}(\boldsymbol{A} - \lambda \boldsymbol{B}) = 0, \tag{3.21}$$

which, for the inviscid case of a horizontal pipe (no source terms), is the same as the stability analysis when we identify $\lambda = \frac{k}{\omega}$.

Once a value for k is chosen (for example through an initial condition consisting of a single wave), ω is determined from the dispersion relation. Subsequently, we choose the initial perturbations such that

$$\left(\boldsymbol{A}^0(i\omega) - \boldsymbol{B}^0(ik) - \boldsymbol{C}^0\right) \boldsymbol{\varepsilon} = 0 \tag{3.22}$$

is satisfied, where $\boldsymbol{\varepsilon} = [\hat{A}_O, \hat{u}_O, \hat{u}_G, \hat{p}]^T$. In practice we fix one of the perturbations, e.g. $\hat{A}_O/A = 10^{-6}$, and determine the other perturbations from the above equation (they can be complex-valued). The complete solution in space and time then reads

$$\boldsymbol{W}(x,t) = \boldsymbol{W}^0 + \mathrm{Re}\left[\boldsymbol{\varepsilon}_1 e^{i(\omega_1 t - kx)} + \boldsymbol{\varepsilon}_2 e^{i(\omega_2 t - kx)}\right], \tag{3.23}$$

and the initial condition used for the numerical simulation follows by setting $t = 0$.

3.2. Compressible flow

The compressible analysis can be performed in a similar manner. The resulting matrices read

$$\boldsymbol{A}^0 = \begin{pmatrix} 1 & 0 & 0 & \frac{A_O}{\rho_O}\frac{\partial \rho_O}{\partial p} \\ -1 & 0 & 0 & \frac{A_G}{\rho_G}\frac{\partial \rho_G}{\partial p} \\ u_O & A_O & 0 & \frac{u_O A_O}{\rho_O}\frac{\partial \rho_O}{\partial p} \\ -u_G & 0 & A_G & \frac{u_G A_G}{\rho_G}\frac{\partial \rho_G}{\partial p} \end{pmatrix}, \tag{3.24}$$

$$\boldsymbol{B}^0 = \begin{pmatrix} u_O & A_O & 0 & \frac{u_O A_O}{\rho_O}\frac{\partial \rho_O}{\partial p} \\ -u_G & 0 & A_G & \frac{u_G A_G}{\rho_G}\frac{\partial \rho_G}{\partial p} \\ u_O^2 + g_n H_O & 2A_O u_O & 0 & \frac{A_O}{\rho_O}(u_O^2\frac{\partial \rho_O}{\partial p} + 1) \\ -u_G^2 + g_n H_G & 0 & 2A_G u_G & \frac{A_G}{\rho_G}(u_G^2\frac{\partial \rho_G}{\partial p} + 1) \end{pmatrix}. \tag{3.25}$$

The dispersion relation is now a *quartic* equation, giving four roots $\omega_{1,2,3,4}$. Two of the roots are close to the ones obtained from the incompressible analysis, the two other roots are much larger and are related to the speed of sound in the gas and liquid.

If the 'full' hydraulic gradient terms, i.e. including derivatives of the density, are employed (see equation (A.7)), $\boldsymbol{B}^0$ changes to

$$\boldsymbol{B}^0 = \begin{pmatrix} u_O & A_O & 0 & \frac{u_O A_O}{\rho_O}\frac{\partial \rho_O}{\partial p} \\ -u_G & 0 & A_G & \frac{u_G A_G}{\rho_G}\frac{\partial \rho_G}{\partial p} \\ u_O^2 + g_n H_O & 2A_O u_O & 0 & \frac{A_O}{\rho_O}(u_O^2\frac{\partial \rho_O}{\partial p} + 1) - \frac{g_n}{\rho_O}\frac{\partial \rho_O}{\partial p}((R-h)A_O - \frac{1}{12}C_{OG}^3) \\ -u_G^2 + g_n H_G & 0 & 2A_G u_G & \frac{A_G}{\rho_G}(u_G^2\frac{\partial \rho_G}{\partial p} + 1) - \frac{g_n}{\rho_G}\frac{\partial \rho_G}{\partial p}((R-h)A_G + \frac{1}{12}C_{OG}^3) \end{pmatrix}. \tag{3.26}$$

From this expression we can easily compare the magnitude of the additional hydraulic gradient term (involving the derivative of the density) with respect to the pressure term:

$$\frac{\frac{g_n}{\rho_G}\frac{\partial \rho_G}{\partial p}((R-h)A_G + \frac{1}{12}C_{OG}^3)}{\frac{A_G}{\rho_G}(u_G^2\frac{\partial \rho_G}{\partial p} + 1)} \approx \frac{g_n R}{c_G^2}. \tag{3.27}$$

The effect of density changes in the hydraulic gradient term compared to the non-conservative pressure term is therefore small.

3.3. Viscous steady state solution

The steady state reference solution around which the equations are linearized cannot be chosen arbitrarily if body forces such as shear stress or gravity are used. Since we will work with periodic boundary conditions when studying interfacial waves, we also assume fully developed flow, and the momentum equations for the steady state solution then simplify to

$$0 = -A_G^0 \frac{\partial p^0}{\partial s} - \tau_{GO}^0 P_{GO}^0 - \tau_G^0 P_G^0 - \rho_G^0 A_G^0 g_s, \tag{3.28}$$

$$0 = -A_O^0 \frac{\partial p^0}{\partial s} + \tau_{GO}^0 P_{GO}^0 - \tau_O^0 P_O^0 - \rho_O^0 A_O^0 g_s. \tag{3.29}$$

These equations can be combined to yield

$$0 = \left(\frac{1}{A_G^0} + \frac{1}{A_O^0} \right) \tau_{GO}^0 P_{GO}^0 + \tau_G^0 \frac{P_G^0}{A_G^0} - \tau_O^0 \frac{P_O^0}{A_O^0} + (\rho_G^0 - \rho_O^0) g_s, \tag{3.30}$$

$$0 = -(A_G^0 + A_O^0) \frac{\partial p^0}{\partial s} - \tau_G^0 P_G^0 - \tau_O^0 P_O^0 - (\rho_G^0 A_G^0 + \rho_O^0 A_O^0) g_s. \tag{3.31}$$

The unknowns in these equations are u_G, u_O, α_O ($\alpha_G = 1 - \alpha_O$), and $\frac{\partial p}{\partial s}$. A typical way to solve these equations is to prescribe the superficial liquid and gas velocities, $u_{sO} = \alpha_O u_O$ and $u_{sG} = \alpha_G u_G$, solve the first equation for α_O, and then the second equation for the pressure drop.

4. Spatial discretization

4.1. Grid layout

We use a staggered grid to discretize the governing equations presented in chapter 2. In a staggered grid the pressure, density, temperature and hold-ups are defined in the centre of a volume, whereas the phase velocities are defined at the faces of a volume. Alternatively, in a finite volume setting it is more natural to say that there are two types of volumes: pressure volumes Ω^p and velocity volumes Ω^u which are shifted half a grid cell with respect to each other. Staggering of the variables leads to a strong coupling between pressure and velocity.

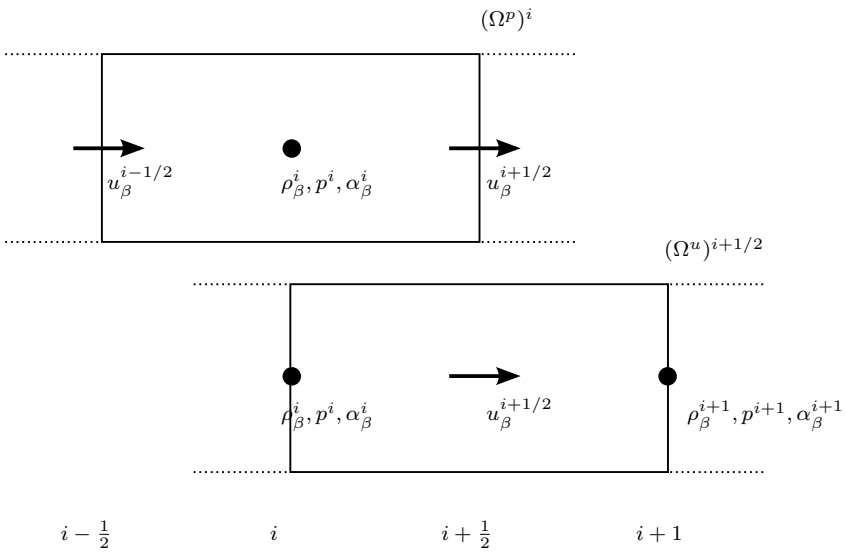

Figure 4.1: Staggered grid layout

4.2. Conservation of mass

Conservation of mass. Consider a 'p-volume' Ω_β^p, with p and ρ defined at the centre of the volume and u at the boundaries. The semi-discrete version of (2.2) reads

$$\frac{\mathrm{d}}{\mathrm{d}t}\left((\Omega_\beta^p)^i \rho_\beta^i\right) + (\rho_\beta A_\beta)^{i+1/2} u_\beta^{i+1/2} - (\rho_\beta A_\beta)^{i-1/2} u_\beta^{i-1/2} = 0. \tag{4.1}$$

The finite volume size is approximated by

$$(\Omega_\beta^p)^i = A_\beta^i (\Delta s^p)^i. \tag{4.2}$$

The face quantity $m_\beta^{i+1/2} = (\rho_\beta A_\beta)^{i+1/2}$ is still to be expressed in terms of the midpoint values, e.g.

$$m_\beta^{i+1/2} = \begin{cases} \frac{1}{2}(m_\beta^i + m_\beta^{i+1}) & \text{central,} \\ m_\beta^i(u_\beta^{i+1/2} > 0) + m_\beta^{i+1}(u_\beta^{i+1/2} < 0) & \text{upwind.} \end{cases} \tag{4.3}$$

Some comments on the use of the upwind approach are given below.

4.3. Conservation of momentum

Conservation of momentum. Consider a 'u-volume' Ω_β^u. The semi-discrete version of (2.4) reads

$$\begin{aligned} &\frac{\mathrm{d}}{\mathrm{d}t}\left((\Omega_\beta^u)^{i+1/2}\rho_\beta^{i+1/2}u_\beta^{i+1/2}\right) + (\rho_\beta A_\beta u_\beta)^{i+1}u_\beta^{i+1} - (\rho_\beta A_\beta u_\beta)^i u_\beta^i = \\ &-A_\beta^{i+1/2}(p^{i+1}-p^i) + LG_\beta^{i+1/2} - \sum_{\substack{\gamma\in O,G,W \\ \gamma\neq\beta}} \tau_{\beta\gamma}^{i+1/2} C_{\beta\gamma}^{i+1/2}(\Delta s^u)^{i+1/2} - (\Omega_\beta^u)^{i+1/2}\rho_\beta^{i+1/2} g_s^{i+1/2}, \end{aligned} \tag{4.4}$$

where

$$(\Omega_\beta^u)^{i+1/2} = A_\beta^{i+1/2}(\Delta s^u)^{i+1/2}, \tag{4.5}$$

and

$$LG_{O,i+1/2} = \left(\rho_O g_n\left[(R-h)A_O - \frac{1}{12}C_{\text{int}}^3\right]\right)_{i+1} - \left(\rho_O g_n\left[(R-h)A_O - \frac{1}{12}C_{\text{int}}^3\right]\right)_i, \tag{4.6}$$

and similarly for the gas phase.

The face quantity $I_\beta^i = (\rho_\beta A_\beta u_\beta)^i$ is still to be expressed in terms of the midpoint values. One can follow the same procedure as for the mass fluxes, i.e. by taking

$$I_\beta^i = \begin{cases} \frac{1}{2}(I_\beta^{i-1/2} + I_\beta^{i+1/2}) & \text{central,} \\ I_\beta^{i-1/2}(u_\beta^{i+1/2} > 0) + I_\beta^{i+1/2}(u_\beta^{i+1/2} < 0) & \text{upwind.} \end{cases} \tag{4.7}$$

However, this approach makes the final stencil larger than necessary: for the central scheme, $I_\beta^{i-1/2}$ requires ρ_β^{i-1}, ρ_β^i and ρ_β^{i+1} (and similar for A_β). Instead one can take:

$$I_\beta^i = \begin{cases} m_\beta^i \frac{1}{2}(u_\beta^{i-1/2} + u_\beta^{i+1/2}) & \text{central,} \\ m_\beta^i u_\beta^{i-1/2}(u_\beta^{i+1/2} > 0) + m_\beta^i u_\beta^{i+1/2}(u_\beta^{i+1/2} < 0) & \text{upwind,} \end{cases} \tag{4.8}$$

where the velocity u_β^i in (4.4) is approximated with central differences. Another alternative, which has the easiest implementation (but introduces more numerical diffusion), is to take

$$I_\beta^i u_\beta^i = \begin{cases} m_\beta^i\left(\frac{1}{2}(u_\beta^{i-1/2} + u_\beta^{i+1/2})\right)^2 & \text{central,} \\ m_\beta^i(u_\beta^{i-1/2})^2(u_\beta^{i+1/2} > 0) + m_\beta^i(u_\beta^{i+1/2})^2(u_\beta^{i+1/2} < 0) & \text{upwind.} \end{cases} \tag{4.9}$$

This is the approach currently used in our two-fluid model. In the simulations in this report only the central scheme has been used. In Compas, on the other hand, an upwind scheme is used.

We note that the 'convective-based' upwinding used in both the mass and momentum equations can contain wiggles (under- and overshoots), especially near sharp gradients. This is due to the fact that an upwind method for a system of nonlinear hyperbolic differential equations should be based on the eigenvalues of the system - the eigenvalues determine the direction in which information travels. In the current approach, we assume that the direction in which information travels is given by the phase velocities, while in reality the direction depends on both the convective velocities and the speed of sound of gas and/or liquid. Determining the eigenvalues (and eigenvectors) can be computationally expensive or cumbersome and is therefore not used.

4.4. Summary of semi-discrete equations

We write the semi-discrete equations symbolically in the following form:

$$\dot{\boldsymbol{U}} = \boldsymbol{F}(\boldsymbol{U}, p), \tag{4.10}$$

$$g(\boldsymbol{U}, p) = 0. \tag{4.11}$$

where $\dot{\boldsymbol{U}} = \mathrm{d}\boldsymbol{U}/\mathrm{d}t$ and $\boldsymbol{F}$ denotes the operator with the discretization of all spatial terms. The components of $\boldsymbol{U}$ are given by

$$U_1 = \rho_G \circ A_G, \tag{4.12}$$

$$U_2 = \rho_O \circ A_O, \tag{4.13}$$

$$U_3 = I_p(\rho_G \circ A_G) \circ u_G, \tag{4.14}$$

$$U_4 = I_p(\rho_O \circ A_O) \circ u_O, \tag{4.15}$$

the components of $\boldsymbol{F}$ by

$$F_1 = -\Omega_p^{-1} D_p \left[I_p(\rho_G \circ A_G) \circ u_G \right], \tag{4.16}$$

$$F_2 = -\Omega_p^{-1} D_p \left[I_p(\rho_O \circ A_O) \circ u_O \right], \tag{4.17}$$

$$F_3 = \Omega_u^{-1} \Big(- D_u \left[\rho_G \circ A_G \circ ((I_u u_G))^2 \right] - (I_p A_G) \circ (D_u p) - (I_p(\rho_G \circ A_G \circ g_n)) \circ (D_u h) \Big) - I_p(\rho_G \circ A_G \circ g_s), \tag{4.18}$$

$$F_4 = \Omega_u^{-1} \Big(- D_u \left[\rho_O \circ A_O \circ ((I_u u_O))^2 \right] - (I_p A_O) \circ (D_u p) - (I_p(\rho_O \circ A_O \circ g_n)) \circ (D_u h) \Big) - I_p(\rho_O \circ A_O \circ g_s), \tag{4.19}$$

and $g(\boldsymbol{U}, p)$ is given by

$$g = A_G + A_O - A. \tag{4.20}$$

There is no interpolation or differentiation involved in evaluating g.

The density is expressed in terms of the pressure via an equation of state (compressible, isothermal), and the interface height in terms of the hold-up fraction via a (non-linear) algebraic relation:

$$\theta = \pi\alpha_O + \left(\frac{3}{2}\pi\right)^{1/3}\left(1 - 2\alpha_O + \alpha_O^{1/3} - (1-\alpha_O)^{1/3}\right), \tag{4.21}$$

$$h = R(1 - \cos\theta). \tag{4.22}$$

The symbol $\circ$ denotes entry-wise multiplication (Hadamard product):

$$U_1 = \rho_G \circ A_G = \begin{pmatrix} (\rho_G A_G)_1 \\ (\rho_G A_G)_2 \\ \vdots \\ (\rho_G A_G)_N \end{pmatrix}. \tag{4.23}$$

In Matlab $\circ$ is denoted by `.*`.

U_1, U_2, F_1, F_2 and g are defined at pressure points. U_3, U_4, F_3 and F_4 are defined at velocity points.

D_p is a differencing operator (matrix) that computes differences from the faces of pressure volumes to midpoints of pressure volumes. Its entries are -1, 1 or 0. I_p is an interpolation operator that interpolates values from pressure midpoints to pressure faces (upwind or central interpolation). When central interpolation is employed, on a uniform grid, its entries are $\frac{1}{2}$ or 0. When periodic boundary conditions are employed we have

$$D_p = \begin{pmatrix} -1 & 1 & & \\ & \ddots & \ddots & \\ & & -1 & 1 \\ 1 & & & -1 \end{pmatrix}, \qquad I_p = \begin{pmatrix} \frac{1}{2} & & & \frac{1}{2} \\ \frac{1}{2} & \frac{1}{2} & & \\ & \ddots & \ddots & \\ & & \frac{1}{2} & \frac{1}{2} \end{pmatrix}. \tag{4.24}$$

In a similar way, D_u is a differencing operator (matrix) that computes differences from velocity faces to velocity midpoints; I_u is an interpolation operator that interpolates values from velocity midpoints to velocity faces. For periodic conditions they read:

$$D_u = \begin{pmatrix} 1 & & & -1 \\ -1 & 1 & & \\ & \ddots & \ddots & \\ & & -1 & 1 \end{pmatrix}, \qquad I_u = \begin{pmatrix} \frac{1}{2} & \frac{1}{2} & & \\ & \ddots & \ddots & \\ & & \frac{1}{2} & \frac{1}{2} \\ \frac{1}{2} & & & \frac{1}{2} \end{pmatrix}. \tag{4.25}$$

5. Temporal discretization

In chapter 4, the continuous system of partial differential equations has been discretized in space, leading to a semi-discrete system of ordinary differential equations supplemented with a constraint. Following the method of lines approach, this system of equations will now be discretized in time. In this chapter we propose a temporal discretization for the semi-discrete equations of the two-fluid model, that is based on the BDF (Backward Differencing Formula) method.

5.1. Introduction

The compressible two-fluid model has four eigenvalues (see section 3.2), two of which are close to the velocity of the gas and liquid, and two of which are much larger, namely close to the acoustic velocities of the gas and liquid. In many cases the fast acoustic waves feature small pressure and velocity perturbations; although one is not interested in resolving these fast transients, the time step associated with resolving these waves is very small. The problem to be solved is therefore called 'stiff': some terms in the differential equations lead to very fast variations, while others are much slower. This means that a time integration method that is able to handle stiff differential equations is required. Such time integration methods are often called L-stable. This is the property that unresolved, high frequency, oscillations will be damped by the time integrator. Note that, apart from the acoustic waves, the volume equation (2.5) which also introduces stiffness. It is a constraint which makes the system of ordinary differential equations a system of differential algebraic equations (DAEs). Such differential algebraic equations generally require the use of a stiff integrator.

The Backward Euler method, which is used in Compas, is an example of a time integration method suitable for stiff systems. Its main drawback is, however, that it is very diffusive. When interpreting Backward Euler as a one-stage Runge-Kutta method, an obvious extension is to add stages to improve the accuracy and reduce the numerical diffusion. For example, the well-known θ-scheme is a two-stage Runge-Kutta method. It has the following properties:

- $\theta = 0$ (Forward Euler): the time step is severely restricted by the stability requirement to capture the acoustic waves (the ones with the largest eigenvalues). Furthermore, the scheme is only first order accurate.
- $\theta = \frac{1}{2}$ (Crank-Nicolson): the scheme is second-order accurate and unconditionally stable. However, when time steps much larger than those associated to the acoustic velocity are taken, oscillations will appear. In other words, perturbations associated with unresolved time scales (stiff terms) lead to oscillations. The method is therefore not L-stable.
- $\theta = 1$ (Backward Euler): this method is very stable and effectively filters out acoustic waves. Stiff terms are handled easily due to the L-stability of the method. However, the method is only first order accurate, leading to strong numerical diffusion.

Physical phenomena tend to get smeared out. Liao et al. [13] and Fullmer et al. [8] use Backward Euler, but require a small time step for their simulations to be accurate.

To summarize, the θ-scheme is not a good candidate for simulating multi-phase flow: it is either too diffusive ($\theta = 1$) or it gives oscillations ($\theta = \frac{1}{2}$).

The solution that we propose is to use a multi-step method instead of a multi-stage method. Backward Euler is namely not only a member of the family of multi-stage (Runge-Kutta) methods, but is also member of the family of multi-step methods. The extension of Backward Euler to second order along the lines of multi-step leads us to consider the second order Backward Differencing Formula (BDF2), a second order method that is especially useful for time integration of stiff differential equations and differential algebraic equations. BDF2 uses three time levels whereas Backward Euler uses two time levels.

5.2. BDF2

We repeat equations (4.10)-(4.11) (leaving out the bold-face notation for vectors):

$$\frac{\mathrm{d}U}{\mathrm{d}t} = F(W,t), \tag{5.1}$$

$$g(W) = 0, \tag{5.2}$$

where U is the vector of conserved variables and W the vector of primitive variables. $F(W,t)$ and $g(W)$ are slightly easier to evaluate than $F(U,t)$ and $g(U,p)$. Most important is, however, that the system of equations which will be discretized in time, is still in conservative form.

The BDF2 method applied to equations (5.1)-(5.2) reads

$$\frac{U^{n+1} - \frac{4}{3}U^n + \frac{1}{3}U^{n-1}}{\Delta t} = \frac{2}{3}F(W^{n+1}, t^{n+1}), \tag{5.3}$$

$$g(W^{n+1}) = 0. \tag{5.4}$$

The θ-method, on the other hand, reads

$$\frac{U^{n+1} - U^n}{\Delta t} = F(\theta W^{n+1} + (1-\theta)W^n, t^n + \theta\Delta t), \tag{5.5}$$

$$g(W^{n+1}) = 0. \tag{5.6}$$

The constraint has to be satisfied at the new time step. In both methods a non-linear system results, that has to be solved iteratively. We concentrate here on BDF2. Introducing the iteration counter m, we write

$$\frac{U^{m+1} - \frac{4}{3}U^n + \frac{1}{3}U^{n-1}}{\Delta t} = \frac{2}{3}F(W^{m+1}, t^{m+1}). \tag{5.7}$$

Furthermore, we write $U^{m+1} = U^m + \Delta U$, and linearise the equations by taking

$$\Delta U = \frac{\partial U}{\partial W} \Delta W, \tag{5.8}$$

$$F(W^{m+1}, t^{n+1}) = F(W^m, t^{n+1}) + \frac{\partial F}{\partial W} \Delta W. \tag{5.9}$$

This leads to the following system that is solved at each time step:

$$\left[\frac{1}{\Delta t} \left(\frac{\partial U}{\partial W} \right)^m - \tfrac{2}{3} \left(\frac{\partial F}{\partial W} \right)^m \right] \Delta W = - \left[\frac{U^m - \frac{4}{3} U^n + \frac{1}{3} U^{n-1}}{\Delta t} - \tfrac{2}{3} F(W^{n+1}, t^{n+1}) \right], \tag{5.10}$$

$$\left(\frac{\partial g}{\partial W} \right)^m \Delta W = -g(W^m), \tag{5.11}$$

or, in other words,

$$A^m \Delta W = f^m. \tag{5.12}$$

This is Newton's method, which converges quadratically if the initial guess is sufficiently close to the solution, and if F is sufficiently differentiable. Upon convergence we have $\|f^m\|_\infty < \epsilon$. Although we solve at each iteration step for ΔW, the final system of equations that is solved is $f = 0$, which equals equation (5.5). Note that it is possible to first write the semi-discrete system in terms of W, by writing

$$\frac{\mathrm{d}W}{\mathrm{d}t} = \left(\frac{\partial U}{\partial W} \right)^{-1} F(W, t), \tag{5.13}$$

and then discretizing this system in time. It is not guaranteed, however, that this set of equations is still conservative, whereas first discretizing in terms of U, and subsequently transforming to W to solve the non-linear equations, keeps this property.

It is also possible to solve the nonlinear system in terms of ΔU, which saves the computation of one Jacobian. This requires that the right-hand side F can be evaluated as function of U, i.e. it requires the transformation from U to W. This transformation is not always straightforward, for example not in case of non-linear equation of state.

Solving system (5.3) has roughly the same computational cost as Backward Euler. From an implementation point of view, BDF2 can be implemented relatively easily in an existing code in which Backward Euler is used (such as Compas), because the only extra required variable is U^{n-1}; the right-hand side is still expressed in terms of $F(W^{n+1})$ only.

The BDF2 method suffers from a start-up problem: at the first time step, when $n = 0$, U^{n-1} is not available. The first time step is therefore computed with the θ-scheme, with θ being either $\frac{1}{2}$ or 1.

5.2.1. Jacobian evaluation

Determining the Jacobians $\left(\frac{\partial U}{\partial W}\right)$ and $\left(\frac{\partial F}{\partial W}\right)$ can be done analytically or by finite difference techniques. We take the latter approach, which is the most flexible and the most easy one to implement (but expensive to evaluate). The only terms that have to be implemented are the functions $U = U(W)$ or $F = F(W)$. Suppose W is a vector of length N, the Jacobian is of size $N \times N$ and is given by

$$J_{i,j} = \frac{F(W_i + \varepsilon\delta_{ij}) - F(W_i)}{W_i + \varepsilon - W_i} = \frac{F(W_i + \varepsilon\delta_{ij}) - F(W_i)}{\varepsilon}, \tag{5.14}$$

where δ_{ij} is the Kronecker delta, and ε a disturbance. A typically useful number for ε is the square root of machine precision multiplied by the maximum value of W [16].

6. Results

6.1. Kelvin-Helmholtz instability

The Kelvin-Helmholtz instability occurs due to an imbalance between shear (viscous) forces and gravity forces (in terms of density differences). In pipelines this instability can lead to the formation of slug flow starting from stratified flow. In the simulations in this section we employ the full compressible model, including the hydraulic gradient terms in compressible form (equation (2.7)). For more detailed simulations and convergence studies with the Rosa code, including comparison with a Discontinuous Galerkin code, we refer to [20].

6.1.1. Inviscid case

We first study the inviscid case, and consider the same problem as considered by Liao et al. [13]. A horizontal pipe of length 1 m is taken ($\varphi = 0$). The density of the gas is given by a perfect gas relation,

$$\rho_G = \frac{p}{c_G^2}, \tag{6.1}$$

where c_G is taken such that for $p = p^0$ we have $\rho_G = 1.1614$ kgm^{-3}. The density of the liquid is constant (incompressible). The velocity difference is 14 ms^{-1}. The values of the other parameters are given in table 6.1.

Liao et al. [13] report that the stability limit is $\Delta U = 16.0768$ ms^{-1}, which means that the model is well-posed and stable for the considered conditions. For larger velocity differences the two-fluid model is ill-posed and numerical simulations have no meaning. The angular frequency (for $k = 2\pi$) is $\omega_1 = 8.05756$ s^{-1}, which is valid for incompressible flow and while using the exact non-linear relation between α and h. If instead one employs Biberg's approximate relation for $\alpha(h)$ [2], which we do in the current simulations, these values slightly change to $\Delta U = 16.0355$ ms^{-1} and $\omega_1 = 8.05755$ s^{-1}. If we furthermore take into account compressibility of the gas, we obtain $\omega_1 = 8.05189$ s^{-1} (note that the critical value of ΔU also changes slightly due to compressibility, which is in contrast to what Bonizzi [5] reports). Note that the second solution to the dispersion relation is $\omega_2 = 4.71950$ s^{-1}.

Table 6.1: Parameter values for inviscid Kelvin-Helmholtz problem.

u_G	u_O	ρ_O	R	p^0	c_G	g
15 ms^{-1}	1 ms^{-1}	1000 kgm^{-3}	0.039 m	10^5 Nm^{-2}	293.43 ms^{-1}	9.8 ms^{-2}

The analytical solution for the compressible case, for the considered conditions, consists of four waves with frequencies $\omega_{1,2,3,4}$, see equation (3.23) and section 3.2. We set

the perturbation of three of these waves to zero, implying that effectively a single wave results. The exact solution is then

$$\boldsymbol{W}(x,t) = \boldsymbol{W}^0 + \mathrm{Re}\left[\boldsymbol{\varepsilon}_1 e^{i(\omega_1 t - kx)}\right], \tag{6.2}$$

and the initial condition follows by taking $t = 0$. $\boldsymbol{\varepsilon}_1$ consists of the following perturbations: we choose the liquid hold-up fraction as $\hat{\alpha}_O = 10^{-6}$, and then the perturbations in gas and liquid velocity follow from the dispersion analysis:

$$\hat{u}_G = 2.7492 \cdot 10^{-5}\ \mathrm{ms}^{-1}, \quad \hat{u}_O = 5.6299 \cdot 10^{-7}\ \mathrm{ms}^{-1}, \quad \hat{p} = -4.3880 \cdot 10^{-4}\ \mathrm{Nm}^{-2}. \tag{6.3}$$

We compare different time integration methods: Backward Euler (BE), Implicit Midpoint (IM), and BDF2. First we perform a qualitative analysis of the liquid hold-up fraction at $t = 1s$, see figure 6.1. A grid with 40 finite volumes is used, and the CFL number is 1 based on the liquid velocity (15 based on the gas velocity). It can be seen that Backward Euler is very diffusive; the peak value in the hold-up fraction has been reduced by more than a factor of 2. BDF2 is clearly less diffusive. Implicit midpoint is the least diffusive, but features a dispersive error (which is especially pronounced on coarse grids). This is a common artefact for wave-type equations, resulting from the use of central schemes in space and time. The evolution of all primary variables is shown in figure 6.2, for the case of the BDF2 scheme.

Secondly, we look at the error convergence as function of time step and mesh spacing, see figure 6.3. The error is defined with respect to the analytical (linearized) solution and the infinity norm is used. The second order accuracy of BDF2 and of implicit midpoint (and of the spatial discretization) is confirmed here, as well as the first order convergence of Backward Euler.

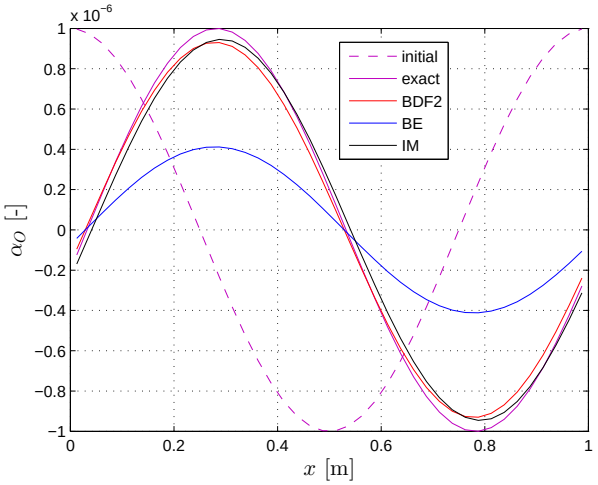

Figure 6.1: Evolution of disturbance in liquid hold-up. Initial solution at $t = 0$s, others at $t = 1$s.

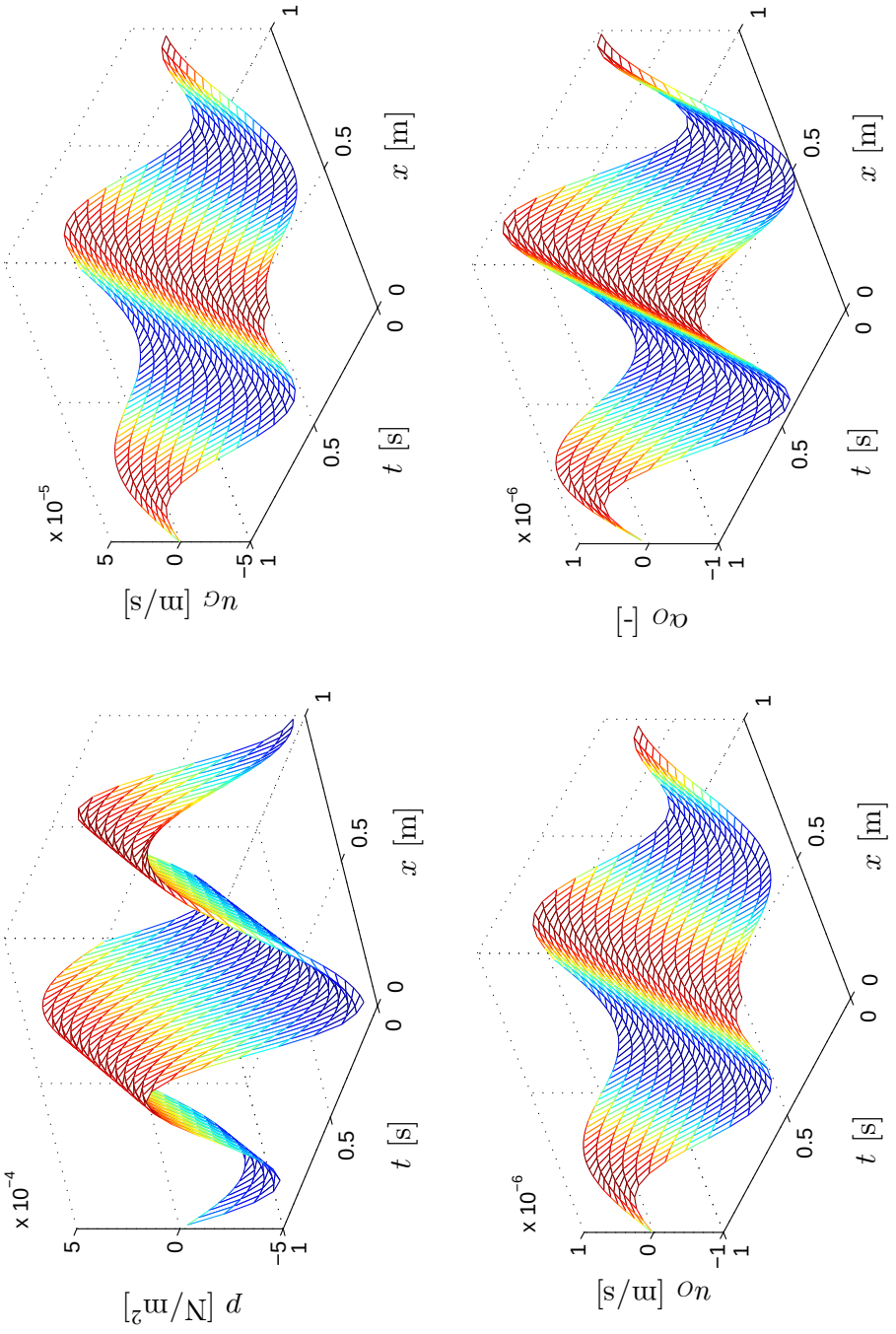

Figure 6.2: Evolution of disturbance in space and time obtained for $N = 40$ with BDF2.

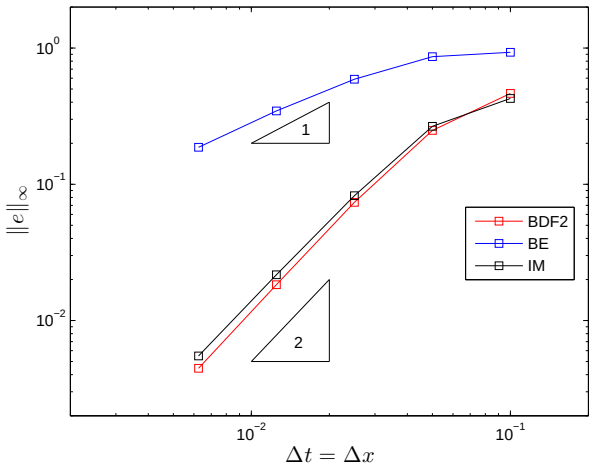

Figure 6.3: Error in α_O at $t = 1$s for different time integration methods, using CFL=1 (based on the liquid velocity).

Acoustic waves

In the previous section we checked the order of accuracy of the scheme by evaluating a single wave with angular frequency ω_1. The velocity of this wave, $(\omega_1/2\pi)$ is of the order of the liquid and gas velocity - see equation (3.19). The eigenvalues of the third and fourth wave are related to the compressibility of the gas (in the incompressible case these eigenvalues are zero, giving infinitely large wave velocities):

$$\frac{\omega_3}{2\pi} = -278.62 \text{ ms}^{-1}, \qquad \frac{\omega_4}{2\pi} = 308.59 \text{ ms}^{-1}, \tag{6.4}$$

which are very close to $u_G - c_G$ and $u_G + c_G$, respectively (note that the liquid is incompressible). If waves with these angular frequencies are also present in the solution, implicit midpoint is prone to oscillations in the pressure because it is not L-stable, but BDF2 effectively filters out these oscillations.

6.1.2. Viscous case

The second case we consider is when shear stresses are activated in the two-fluid model. This is a much more interesting case, because for certain conditions the two-fluid model is *unstable while well-posed*, and we can study the growth of waves that might eventually lead to slug formation.

Linear regime

When adding shear stress terms in the equations, the total momentum of the flow (with periodic boundary conditions) is not conserved, and a body force is necessary to drive

the flow. Liao [13] gave the pipe a downward inclination to achieve this, but this has the disadvantage that it also affects the magnitude of the hydraulic gradient term. Instead we add a driving pressure gradient to the equations, which is such that the friction terms are balanced in the steady state case (see section 3.3). We choose $u_O = 1$ ms^{-1}, $\alpha_O = 0.5$, and then the viscous (turbulent) steady state equations are solved to give

$$u_G = 13.9784 \text{ ms}^{-1}, \qquad \frac{\partial p}{\partial s} = -76.3963 \text{ Pa m}^{-1}. \tag{6.5}$$

See table 6.2 for parameter values not yet listed in table 6.1.

Table 6.2: Parameter values for viscous Kelvin-Helmholtz problem.

u_G	u_O	μ_G	μ_O	friction
13.9784 ms^{-1}	1 ms^{-1}	$1.8 \cdot 10^{-5}$ Pa s	$8.9 \cdot 10^{-4}$ Pa s	turbulent

The velocity difference between the phases is well below the critical limit, which means that the equations are well-posed. Linear stability analysis gives the following (compressible) unstable frequency (for $k = 2\pi$):

$$\omega_1 = 8.4437 - 0.3645i \text{ s}^{-1} \tag{6.6}$$

The negative imaginary part makes the solution unstable (exponential growth in time). The initial perturbation is again given by $\hat{\alpha}_O = 10^{-6}$, and the other perturbations follow as

$$\begin{aligned} \hat{u}_G &= (2.5316 + 0.0125i) \cdot 10^{-5} \text{ ms}^{-1}, \\ \hat{u}_O &= (6.8770 - 1.1601i) \cdot 10^{-7} \text{ ms}^{-1}, \\ \hat{p} &= (-3.7183 - 0.6765i) \cdot 10^{-4} \text{ Pa}. \end{aligned} \tag{6.7}$$

We compare the exact growth rate as given by equation (6.6) with the growth rate predicted by the simulation. The numerical growth rate for a grid with N volumes is calculated from the maximum value of the liquid hold-up fraction at two time instances:

$$\omega_N = \frac{\ln(\max \alpha_O(t_2)) - \ln(\max \alpha_O(t_1))}{t_2 - t_1}, \tag{6.8}$$

where we have taken $t_1 = 0$ s and $t_2 = 10$ s. Figure 6.4a shows the convergence towards the analytical growth rate with increasing number of finite volumes. Figure 6.4b shows a similar result, but here the difference between the analytical and numerical solution is displayed on a log-log scale. The slope of the error curve confirms second order convergence of the presented method, in both space and time (since we work at a fixed CFL number).

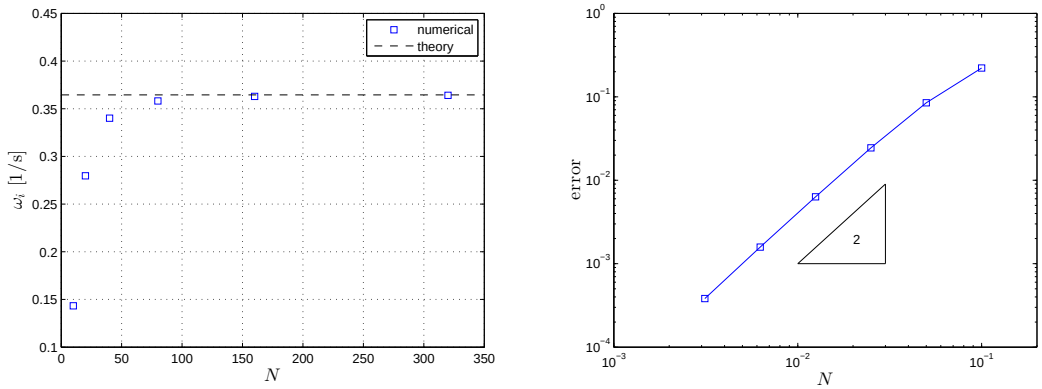

(a) Absolute value of growth rate. **(b)** Error.

Figure 6.4: Growth rate as function of mesh size and convergence to theoretical value, using Implicit Midpoint.

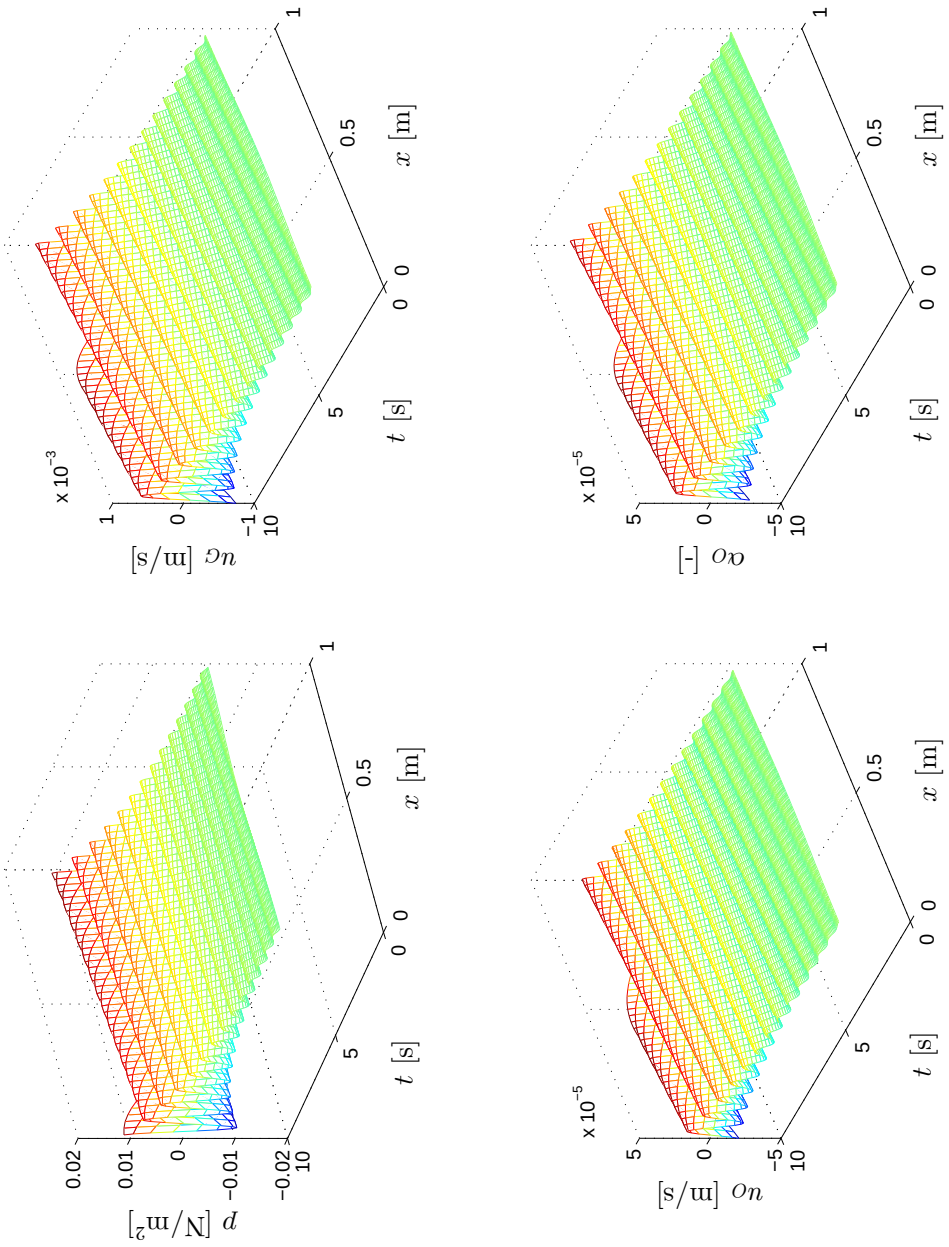

Figure 6.5: Complete solution in space and time obtained for $N = 40$ using Implicit Midpoint.

Non-linear effects

As a further test we investigate what happens when the perturbation is much larger and the simulation enters the non-linear regime. The linear stability analysis is now no longer valid and we only perform a qualitative analysis. The results have been obtained with the BDF2 scheme, with $N = 40$ and CFL=$\frac{1}{2}$ based on the initial liquid velocity of 1 ms^{-1}. Figure 6.6a shows that the growth rate of the solution departs from the theoretical linear one: the growth rate becomes larger than the theoretical linear value and then saturates. A similar effect is reported in [13]. The liquid hold-up fraction α_O as a function of space is shown for different time instances in figure 6.7. The non-linear behaviour can be observed from the fact that the profiles depart from the sinusoidal initial condition. When time increases, non-linear effects become increasingly important: figure 6.6b shows that the number of iterations that the Newton solver requires at each time step to solve the non-linear system of equations increases with time. Around $t = 7.9$ s, Newton's method did not converge within 10 iterations and computations were stopped. Figure 6.6b shows that at this time the liquid starts to touch the upper pipe wall, and the flow becomes locally single phase. The gas velocity increases rapidly in the region of large liquid hold-up fractions (up to 40 ms^{-1}).

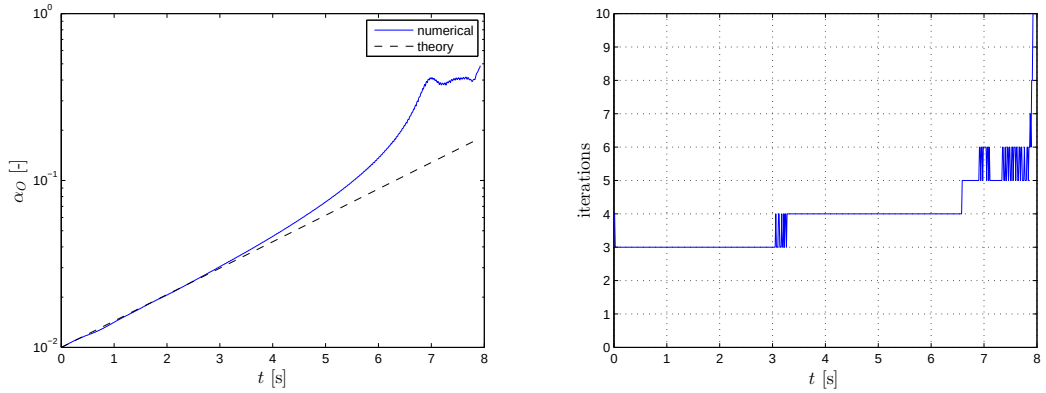

(a) Maximum liquid hold in time.

(b) Number of iterations of Newton's method.

Figure 6.6: Nonlinear effects in viscous KH simulation.

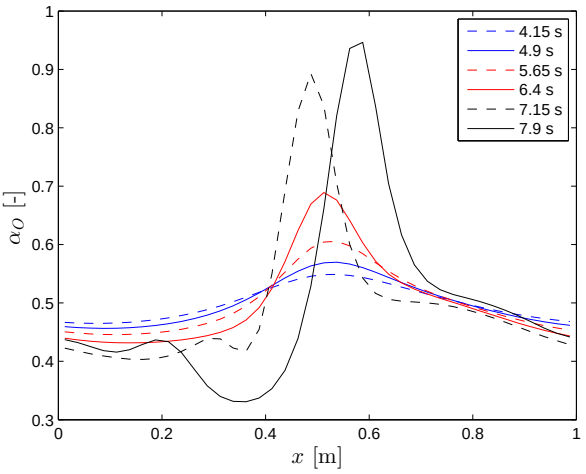

Figure 6.7: Liquid hold-up fraction α_O at different time instances.

6.2. Dam-break problem (shallow water equations)

As described in appendix B, the shallow water equations are a special case of the two-fluid model obtained when assuming that the gas above the liquid is at rest and at constant pressure, i.e. open channel flow. The problem we study here is the *dam-break problem*, for which an analytical solution exists. A dam, initially separating two horizontal levels of liquid, bursts, and a left- and right-moving wave appear. The dam-break problem is a relevant test problem, not only because a 1D (unsteady) analytical solution is available, but also because 2D and 3D (steady) solutions exist, known as the Benjamin bubble. These latter solutions can be used at a later stage as a means to validate how well the one-dimensional equations approximate the actual 2D or 3D solution.

In the Rosa code the shallow water equations are effectively recovered when a channel with a large height and a gas with a much lower density than the oil is taken. We take a channel height of 10 m, and an initial liquid layer height that varies smoothly (according to a hyperbolic tangent function) from 0.75 to 0.25 m. The smooth variation is necessary to prevent oscillations that would otherwise result due to the use of central differencing schemes. The exact solution features a (left-running) expansion wave and a (right-running) shock wave. The intermediate state, at the position where the dam was present, is given by equations (B.8) - (B.7). For the case under consideration the solution is given by

$$h_m \approx 0.462 \text{ m}, \qquad u_m \approx 1.167 \text{ ms}^{-1}. \tag{6.9}$$

The simulation domain is 10 m long, and 40 finite volumes are used ($\Delta x = 0.25$ m); the time step is $\Delta t = 0.025$ s. Backward Euler is used as a time integration method in order to add sufficient diffusion to prevent the appearance of oscillations arising from the

use of a central scheme for the spatial discretization of the convective terms. It is possible to use higher order methods in combination with a flux or slope limiter to prevent oscillations.

The results in figure 6.8 show the emergence of a right-moving shock and a left-moving expansion. The results are smeared out due to the use of Backward Euler and a smooth initial condition. The deviation of the pressure from the background pressure (1 bar) is shown (units: Pascal), and is very small. This is consistent with the shallow water equations, in which the pressure term is neglected.

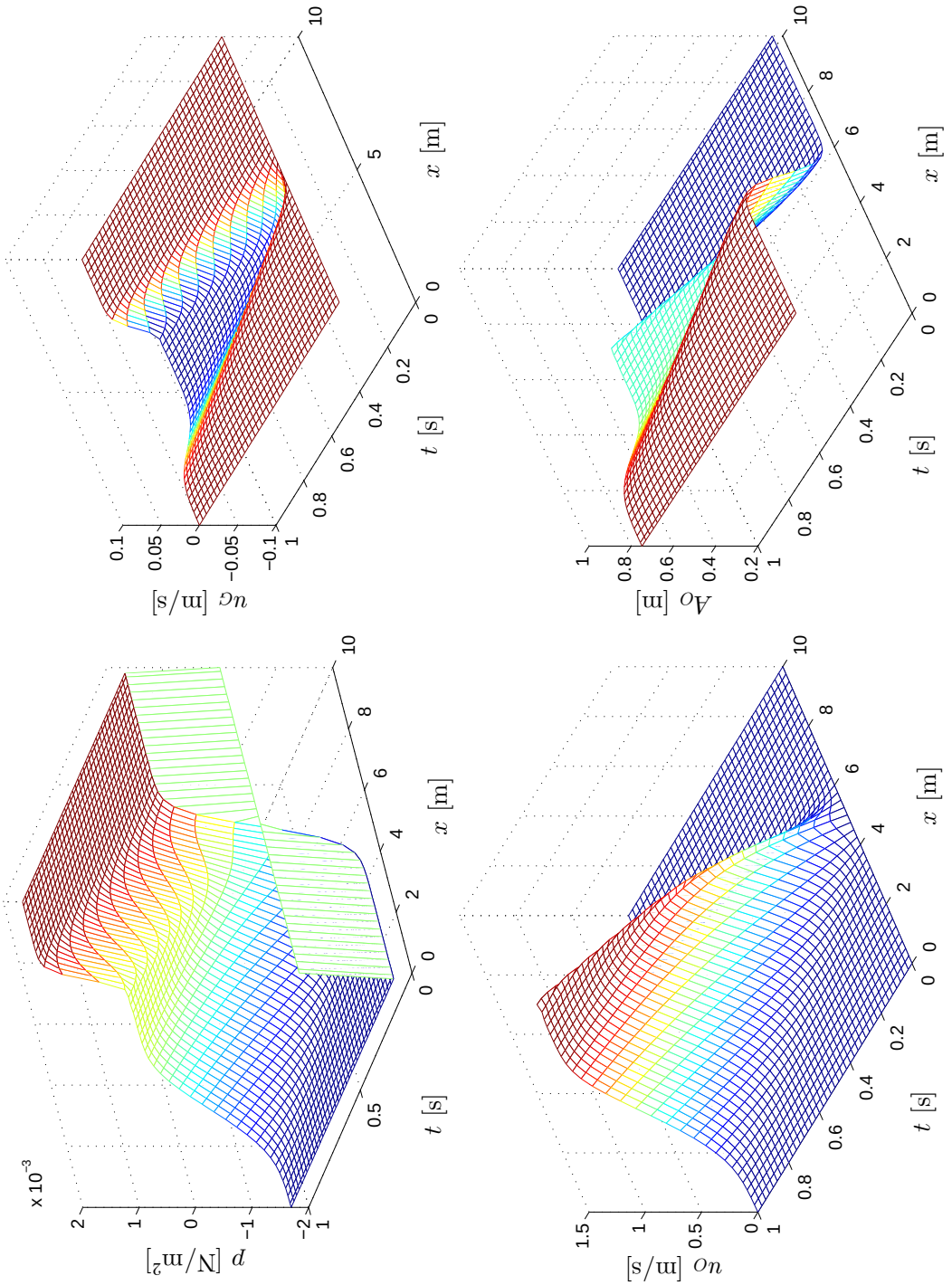

Figure 6.8: Solution for dam-break problem starting from a smooth initial condition and using Backward Euler.

7. Conclusions

In this report we have presented a second order accurate method for simulating stratified flows as modelled by the two-fluid model. For the spatial derivatives, second order central differences have been used, which are suitable as long as sharp discontinuities do not develop. For the integration in time, the use of the second order Backward Differencing Formula (BDF2) is proposed as an alternative to the commonly used Backward Euler method, having similar stability properties and computational cost, but being more accurate. BDF2 effectively filters acoustic waves when 'large' time steps are employed (i.e. based on convective velocities), and resolves them when time steps based on acoustic velocities are employed.

The method has been verified by a quantitative comparison with an analytical solution for the Kelvin-Helmholtz instability and a qualitative comparison with an analytical solution for the dam-break problem. The Kelvin-Helmholtz study confirms the second order accuracy in both the inviscid and viscous case. In the viscous case the equations are well-posed but unstable and the correct growth rate is obtained. Upon continued simulation outside the linear regime, wave steepening is observed, which eventually develops into slug flow.

The main purpose of the discretization developed here is to replace the drift-flux model in Compas by the two-fluid model. At the same time, the developed prototype Matlab code *Rosa* offers a sandbox environment in which a number of algorithms, planned to be put into Compas' new numerical scheme, can be studied:

- Including hydraulic gradient terms in the equations. These terms are the mechanism behind the appearance of interfacial waves (Kelvin-Helmholtz instabilities).
- Replacing the volume constraint (sum of hold-ups equals 1) by a pressure equation in such a way that the volume error remains zero.
- Deriving boundary treatment based on a local eigenvalue analysis of the governing equations.
- Investigating algorithms for bypass pigging, in particular friction models.
- Coupling to a reservoir model to study well-reservoir interaction.

Appendix A.

Hydraulic gradients

A.1. Pipe flow

In [18] the hydraulic gradient terms were derived by integrating the hydrostatic pressure variation over the cross-sectional area of a phase. This stems from the fact that the pressure term in the two-fluid model reads

$$-\frac{\partial}{\partial s}\left(\int_{A_\beta} p_\beta \,\mathrm{d}A\right) + p_{\text{int}}\frac{\partial A_\beta}{\partial s}, \tag{A.1}$$

where the pressure $p_\beta(s,h,t)$ is still a function of the normal coordinate h, and $p_{\text{int}}(s,t)$ is the interface pressure. p_{int} is the pressure that will be the unknown in the resulting system of equations. $p_\beta(s,h,t)$ can be expressed in terms of p_{int} by using the momentum equation in normal direction:

$$p_\beta(s,h,t) = p_{\text{int}}(s,t) - \rho_\beta(s,t) g_n (h - h_{\text{int}}(s,t)), \tag{A.2}$$

where $g_n(s) = g\cos\varphi(s)$.

There are different ways to proceed to derive the hydraulic gradients:

1. Substitute expression (A.2) into (A.1) and integrate over the cross-section.
2. Write (A.1) as
$$-\int_{A_\beta} \frac{\partial p_\beta}{\partial s}\,\mathrm{d}A \tag{A.3}$$
and then substitute (A.2).

The second approach is the approach taken in [18]. Here we will instead take the first approach, because it allows us to obtain the hydraulic gradient terms in conservative form, which are more suitable for discretization with the finite volume method. We will show that both approaches are equivalent on the continuous level.

The first approach leads to (we consider only the liquid phase)

$$\begin{aligned} -\frac{\partial}{\partial s}\left(\int_{A_O} p_{\text{int}} - \rho_O g_n (h - h_{\text{int}})\,\mathrm{d}A\right) + p_{\text{int}}\frac{\partial A_O}{\partial s} = \\ - A_O\frac{\partial p_{\text{int}}}{\partial s} + \boxed{\frac{\partial}{\partial s}\left(\rho_O g_n\left[(R - h_{\text{int}})A_O - \frac{1}{12}C_{\text{int}}^3\right]\right)}. \end{aligned} \tag{A.4}$$

The boxed term is the hydraulic gradient term that enters in the governing equations. Note that the integral has been evaluated by taking:

$$\begin{aligned} \int_{A_O} h\,\mathrm{d}A &= 2\int_\theta R(1-\cos\theta)R^2\sin^2\theta\,\mathrm{d}\theta \\ &= R^3\left[\theta - \frac{1}{2}\sin 2\theta - \frac{2}{3}\sin^3\theta\right]_0^{\theta_{OG}} = RA_O - \frac{1}{12}C_{OG}^3. \end{aligned} \tag{A.5}$$

Similarly, the contribution to the gas momentum equation is

$$\begin{aligned}\int_{A_G} h\,\mathrm{d}A &= 2\int_{\theta} R(1-\cos\theta)R^2\sin^2\theta\,\mathrm{d}\theta \\ &= R^3\left[\theta - \frac{1}{2}\sin 2\theta - \frac{2}{3}\sin^3\theta\right]_{\theta_{OG}}^{\pi} = RA_G + \frac{1}{12}C_{OG}^3.\end{aligned} \tag{A.6}$$

The form (A.4) is in conservative form and suitable for discretization with the finite volume method.

The second approach gives (see [18])

$$\begin{aligned}-\int_{A_O(s)} \frac{\partial p_O}{\partial s}\mathrm{d}A &= -\int_{A_O(s)} \frac{\partial}{\partial s}\left(p_{\text{int}} - \rho_O g_n (h - h_{\text{int}})\right)\mathrm{d}A \\ &= -A_O\frac{\partial p_{\text{int}}}{\partial s} - \rho_O g_n A_O \frac{\partial h_{\text{int}}}{\partial s} + \frac{\partial}{\partial s}\left(\rho_O g_n\right)\left[(R-h_{\text{int}})A_O - \frac{1}{12}C_{\text{int}}^3\right].\end{aligned} \tag{A.7}$$

We now show that both approaches are equivalent. The hydraulic gradient terms of the first approach are written as

$$\begin{aligned}\frac{\partial}{\partial s}\left(\rho_O g_n\left[(R-h_{\text{int}})A_O - \frac{1}{12}C_{\text{int}}^3\right]\right) = \\ \rho_O g_n A_O \frac{\partial}{\partial s}(R-h_{\text{int}}) + \rho_O g_n \frac{\partial A_O}{\partial s}(R-h_{\text{int}}) + A_O(R-h_{\text{int}})\frac{\partial}{\partial s}\left(\rho_O g_n\right) \\ - \frac{\partial}{\partial s}\left(\rho_O g_n\right)\frac{1}{12}C_{\text{int}}^3 - \frac{\partial}{\partial s}\left(\frac{1}{12}C_{\text{int}}^3\right)\rho_O g_n.\end{aligned} \tag{A.8}$$

The first, second and last terms cancel because of a geometric identity:

$$A_O\frac{\partial R}{\partial s} + \frac{\partial A_O}{\partial s}(R-h_{\text{int}}) - \frac{\partial}{\partial s}\left(\frac{1}{12}C_{\text{int}}^3\right) = 0. \tag{A.9}$$

This can be proven by expressing A_O, h_{int} and C_{int} in terms of R and θ_{int} (see [18]). The first approach can therefore be written as

$$\begin{aligned}\frac{\partial}{\partial s}\left(\rho_O g_n\left[(R-h_{\text{int}})A_O - \frac{1}{12}C_{\text{int}}^3\right]\right) = -\rho_O g_n A_O\frac{\partial h_{\text{int}}}{\partial s} + \\ A_O(R-h_{\text{int}})\frac{\partial}{\partial s}\left(\rho_O g_n\right) - \frac{\partial}{\partial s}\left(\rho_O g_n\right)\frac{1}{12}C_{\text{int}}^3,\end{aligned} \tag{A.10}$$

which is equivalent to the hydraulic gradient terms in (A.7). In Henkes [9] the last two terms that involve density variations are not present. This is therefore effectively the incompressible model, which is widely used in the literature, and which features only the term

$$-\rho_O g_n A_O\frac{\partial h_{\text{int}}}{\partial s}. \tag{A.11}$$

A.2. Channel flow

In the case of channel flow, the evaluation of the integrals is slightly easier:

$$\begin{aligned}\frac{\partial}{\partial s}\left(\int_{A_O}\rho_O g_n(h-h_{\text{int}})\,\mathrm{d}A\right) &= \frac{\partial}{\partial s}\left(\rho_O g_n\left[\frac{1}{2}h^2-h_{\text{int}}h\right]_0^{h_{\text{int}}}\right)\\ &= -\frac{\partial}{\partial s}\left(\frac{1}{2}\rho_O g_n h_{\text{int}}^2\right).\end{aligned} \tag{A.12}$$

For the gas phase we have

$$\frac{\partial}{\partial s}\left(\int_{A_G}\rho_G g_n(h-h_{\text{int}})\,\mathrm{d}A\right) = -\frac{\partial}{\partial s}\left(\frac{1}{2}\rho_G g_n(H-h_{\text{int}})^2\right), \tag{A.13}$$

where H is the channel height.

Appendix B.

Shallow water equations

In certain circumstances the equation for the liquid phase can be simplified. If the effect of the gas on the liquid is small, which can be the case if the liquid phase is not restricted by the pipeline geometry (e.g. the flow of a river in a quiescent atmosphere), we obtain the following equations:

$$\frac{\partial}{\partial t}\left(\rho_O A_O\right) + \frac{\partial}{\partial s}\left(\rho_O u_O A_O\right) = 0, \tag{B.1}$$

$$\frac{\partial}{\partial t}\left(\rho_O u_O A_O\right) + \frac{\partial}{\partial s}(\rho_O u_O^2 A_O) = -\rho_O g A_O \frac{\partial A_O}{\partial s}. \tag{B.2}$$

Note that we assumed a horizontal channel (taking $A_O = h$), and ignored the shear stress. Since $\rho_O = \rho_O(p) =$ constant, one can divide by the density and obtain the following formulation:

$$\frac{\partial h}{\partial t} + \frac{\partial}{\partial s}\left(hu\right) = 0, \tag{B.3}$$

$$\frac{\partial}{\partial t}\left(hu\right) + \frac{\partial}{\partial s}\left(hu^2 + \frac{1}{2}gh^2\right) = 0. \tag{B.4}$$

These equations are known as the *shallow water equations* (SWE). The pressure has disappeared from the equations due to the assumption of uniform atmospheric gas pressure, and at the same time the volume equation has disappeared. This corresponds to the observation that the volume equation is an equation for the pressure.

The shallow water equations do, in general, not hold for multiphase flow in pipelines, because the gas phase is compressible and its pressure is not uniform. The shallow water equations furthermore do no guarantee that the actual liquid level h will be such that $A_L \leq A$.

Note that the SWE can be interpreted in terms of the single phase Euler equations, written as

$$\frac{\partial \rho}{\partial t} + \frac{\partial}{\partial s}\left(\rho u\right) = 0, \tag{B.5}$$

$$\frac{\partial}{\partial t}\left(\rho u\right) + \frac{\partial}{\partial s}\left(\rho u^2 + p(\rho)\right) = 0, \tag{B.6}$$

when the isentropic relation $p(\rho) = C\rho^\gamma$ with $\gamma = 2$ and $C = \frac{1}{2}g$ is employed, and the height h is interpreted as the density.

For simple initial conditions the solution of these hyperbolic partial differential equations can be obtained by solving a Riemann problem. The SWE feature two distinct eigenvalues, $\lambda_{1,2} = u \pm \sqrt{gh}$, associated with the wave speeds. Solutions feature a combination of expansion and shock waves (there are no contact discontinuities). See for example [12]

for a detailed explanation. A well-known problem that can be solved exactly is the dam-break problem: a dam at $x = 0$ separates a stationary fluid, having height h_l on the left side of the dam, and height h_r on the right side. When the dam is removed, a shock and and an expansion wave result. The exact solution for the intermediate state is obtained by solving

$$u_l + 2(\sqrt{gh_l} - \sqrt{gh_m}) = u_r + (h_m - h_r)\sqrt{\frac{g}{2}\left(\frac{1}{h_m} + \frac{1}{h_r}\right)}, \tag{B.7}$$

and u_m follows as

$$u_m = u_O + 2(\sqrt{gh_l} - \sqrt{gh_m}). \tag{B.8}$$

For $h_l > h_r$ the solution always consists of an expansion wave and a shock wave. In the special case $h_r = 0$ (dry ground right of the dam), there is *no shock*, but only an expansion wave whose head is moving with speed $2\sqrt{gh_l}$ and whose tail is moving with speed $-\sqrt{gh_l}$. The analytical solution for $-\sqrt{gh_l}t < x < 2\sqrt{gh_l}t$ is [3]

$$h(x,t) = \frac{h_l}{9}\left(2 - \frac{x}{\sqrt{gh_l}t}\right)^2, \tag{B.9}$$

and

$$u(x,t) = \frac{2}{3}\left(\frac{x}{t} + \sqrt{gh_l}\right). \tag{B.10}$$

h and hu are continuous throughout the domain, but u jumps at $x = 2\sqrt{gh_l}t$.

Appendix C.

Code structure

The Rosa code is written in Matlab and available on the Team Foundation Server in the folder
`/ProcessSimulationTools/Compas/trunk/src/MatlabSandbox/1D_stratified_isothermal`
The simulations in this report have been obtained with changeset `163381`. The layout of the algorithm in terms of pseudo-code is shown below in algorithm 1.

Algorithm 1: Two-fluid model code structure

initialization of parameters and constants
create computational grid → `create_grid`
set up spatial discretization → `matrices`
stability analysis → `VKH2`, `viscous_steady_state`, `friction`
initial condition

time integration:
while $t < t_{end}$ **do**
  perform one time step - solve nonlinear system:
  while *residual* > *threshold* **do**
    determine Jacobians → `Jacobian`
    get right hand side $\boldsymbol{F}$ → `FW`
    solve linear system for $\delta\boldsymbol{W}$
    update $\boldsymbol{W}$
  end
end
post-processing

References

[1] D. Barnea and Y. Taitel. Interfacial and structural stability of separated flow. *International Journal of Multiphase Flow*, 20(94):387–414, 1994.

[2] D. Biberg. An explicit approximation for the wetted angle in two-phase stratified pipe flow. *The Canadian Journal of Chemical Engineering*, 77(3):1221–1224, 1999.

[3] J. Billingham and A.C. King. *Wave motion*. Cambridge University Press, 2000.

[4] C.P.A. Blom, R.A.W.M. Henkes, A.J.N. Vreenegoor, and G. Haandrikman. Numerics for the dynamic transition from stratified flow to slug flow. Shell Report OP.99.20233, 1999.

[5] M. Bonizzi. *Transient one-dimensional modelling of multiphase slug flows*. PhD thesis, Imperial College, 2003.

[6] M. Bonizzi, P. Andreussi, and S. Banerjee. Flow regime independent, high resolution multi-field modelling of near-horizontal gas-liquid flows in pipelines. *International Journal of Multiphase Flow*, 35(1):34–46, January 2009.

[7] S. Evje and T. Flåtten. Hybrid flux-splitting schemes for a common two-fluid model. *Journal of Computational Physics*, 192(1):175–210, 2003.

[8] W.D. Fullmer, V.H. Ransom, and M.A. Lopez de Bertodano. Linear and nonlinear analysis of an unstable, but well-posed, one-dimensional two-fluid model for two-phase flow based on the inviscid Kelvin-Helmholtz instability. *Nuclear Engineering and Design*, 268:173–184, November 2014.

[9] R.A.W.M. Henkes, A.J.N. Vreenegoor, and G. Haandrikman. Threephase flow model for the stratified flow of water, oil and gas in pipelines. Shell Report OP.98.20590, 1998.

[10] H. Holmås. *Numerical simulation of waves in two-phase pipe flow using 1D two-fluid models*. PhD thesis, 2008.

[11] R.I. Issa and M.H.W. Kempf. Simulation of slug flow in horizontal and nearly horizontal pipes with the two-fluid model. *International Journal of Multiphase Flow*, 29(1):69–95, 2003.

[12] R.J. LeVeque and Z. Li. Immersed interface methods for Stokes flow with elastic boundaries or surface tension. *SIAM Journal on Scientific Computing*, 18(3):709–735, 1997.

[13] J. Liao, R. Mei, and J.F. Klausner. A study on the numerical stability of the two-fluid model near ill-posedness. *International Journal of Multiphase Flow*, 34(11):1067–1087, 2008.

[14] M. Montini. *Closure relations of the one-dimensional two-fluid model for the simulation of slug flows*. PhD thesis, Imperial College, 2011.

[15] C. Omgba-Essama. *Numerical Modelling of Transient Gas-Liquid Flows (Application to Stratified and Slug Flow Regimes)*. PhD thesis, Cranfield University, 2004.

[16] A. Prosperetti and G. Tryggvason. *Computational methods for multiphase flow*. Cambridge University Press, 2007.

[17] R.W. Lyczkowski and D. Gidaspow and C.W. Solbrig and E.D. Hughes. Char-

acteristics and Stability Analyses of Transient One-Dimensional Two-Phase Flow Equations and Their Finite Difference Approximations. *Nuclear Science and Engineering*, 66(3):378–396, 1978.

[18] B. Sanderse. Governing equations of single- and multi-phase flow in one-dimensional pipelines. Shell Report SR.13.13992, 2013.

[19] H.B. Stewart and B. Wendroff. Two-phase flow: models and methods. *Journal of Computational Physics*, 56:363–409, 1984.

[20] J.S.B. van Zwieten, B. Sanderse, M.H.W. Hendrix, C. Vuik, and R.A.W.M. Henkes. Efficient simulation of one-dimensional two-phase flow with a new high-order discontinuous galerkin method. Technical Report Reports of the Delft Institute of Applied Mathematics 15-07, Delft University of Technology, 2015.

[21] A.J.N. Vreenegoor, R.A.W.M. Henkes, and G. Haandrikman. Improvement of Shell's transient multiphase flow models: A stratified-wavy/slug flow model derived from first principles. Shell Report OP.98.20051, 1998.

[22] T. Wangensteen. *Mixture-Slip Flux Splitting for the Numerical Computation of 1D Two Phase Flow*. PhD thesis, Norwegian University of Science and Technology (NTNU), 2010.

Bibliographic information

Classification	Restricted
Report Number	SR.16.10592
Title	Development of a two-fluid model for dynamic multiphase pipeline simulations
Subtitle	Introduction and description of the prototype code Rosa
Authors	B. Sanderse (PTE/EPFA)
Keywords	two-fluid model, stratified flow, Kelvin-Helmholtz, stability analysis, shallow water equations
Issue Date	March 2016
Period of work	January-December 2015
US Export Control	Non US — Public Domain
WBSE Code	ZZPT/021835/010202, ZZPT/015243/010501
Reviewed by	R.A.W.M. Henkes
Approved by	R.A.W.M. Henkes
Sponsoring Company/ Customer	
Spons./Cust. Address	
Issuing Company	Shell Global Solutions International B.V., Amsterdam P.O. Box 38000 1030 BN Amsterdam The Netherlands

Report distribution

Electronic distribution (PDF)

Name, Company, Ref. Ind.	
PT Information Services, PTT/TIKE, PT-Information-Services@Shell.com	PDF
Dewan, Ashok K GSUSI-PTT/EPEN	PDF
Fransen, Maurice ALJ GSNL-PTE/EPFA	PDF
Groote, Gijs A GSNL-PTE/EPFA	PDF
Haverkort, Willem W GSNL-PTI/GF	PDF
Henkes, Ruud AWM GSNL-PTE/EPFA	PDF
IJzermans, Rutger PTIN-PTI/GF	PDF
Kerem, Murat GSNL-PTE/EPFA	PDF
Kramer, Joanne G GSNL-PTE/EPFA	PDF
Kreeft, Jasper J GSNL-PTI/GF	PDF
Mantravadi, Vasudeva Kumar PTIN-PTT/EPEN	PDF
Moeleker, Piet PTIN-PTE/PPFA	PDF
Pagliuca, Giuseppe GSNL-PTE/EPFA	PDF
Rosen Esquivel, Patricio I GSNL-PTE/EPFA	PDF
Sanderse, Benjamin GSNL-PTE/EPFA	PDF
Schiferli, Wouter GSNL-PTE/EPFA	PDF
T'Joen, Christophe G GSNL-PTE/EPFA	PDF
van Dijk, Menno A GSNL-PTE/EPFA	PDF
Vreenegoor, Loek JN GSNL-PTE/EPFA	PDF

Principal typesetting performed with LaTeX system (MiKTeX) using the PTreport2015.cls class based on the KOMA-Script with the necessary modifications to match the Shell Projects and Technology house style.

The PTreport2015.cls class file is written and maintained by IDLTeX (www.idltex.com). All rights reserved.